International Journal of Solids and Structures 88–89 (2016) 227–247

Contents lists available at ScienceDirect

International Journal of Solids and Structures

journal homepage: www.elsevier.com/locate/ijsolstr

A thermodynamically consistent plastic-damage framework for localized failure in quasi-brittle solids: Material model and strain localization analysis

Jian-Ying Wu [a,*], Miguel Cervera [b]

[a] State Key Laboratory of Subtropical Building Science, South China University of Technology, Guangzhou 510641, China
[b] CIMNE, Technical University of Catalonia, Edificio C1, Campus Norte, Jordi Girona 1-3, Barcelona 08034, Spain

ARTICLE INFO

Article history:
Received 27 August 2015
Revised 3 March 2016
Available online 24 March 2016

Keywords:
Localized failure
Damage
Plasticity
Fracture
Constitutive behavior
Strain localization
Concrete

ABSTRACT

Aiming for the modeling of localized failure in quasi-brittle solids, this paper addresses a thermodynamically consistent plastic-damage framework and the corresponding strain localization analysis. A unified elastoplastic damage model is first presented based on two alternative kinematic decompositions assuming infinitesimal deformations, with the evolution laws of involved internal variables characterized by a dissipative flow tensor. For the strong (or regularized) discontinuity to form in such inelastic quasi-brittle solids and to evolve eventually into a fully softened one, a novel strain localization analysis is then suggested. A kinematic constraint more demanding than the classical discontinuous bifurcation condition is derived by accounting for the traction continuity and the loading/unloading states consistent with the kinematics of a strong (or regularized) discontinuity. More specifically, the strain jumps characterized by Maxwell's kinematic condition have to be completely inelastic (energy dissipative). Reproduction of this kinematics implies vanishing of the aforesaid dissipative flow tensorial components in the directions orthogonal to the discontinuity orientation. This property allows naturally developing a localized plastic-damage model for the discontinuity (band), with its orientation and the traction-based failure criterion consistently determined *a posteriori* from the given stress-based counterpart. The general results are then particularized to the 2D conditions of plane stress and plane strain. It is found that in the case of plane stress, strain localization into a strong (or regularized) discontinuity can occur at the onset of strain softening. Contrariwise, owing to an extra kinematic constraint, in the condition of plane strain some continuous inelastic deformations and substantial re-orientation of principal strain directions in general have to take place in the softening regime prior to strain localization. The classical Rankine, Mohr–Coulomb, von Mises (J_2) and Drucker–Prager criteria are analyzed as illustrative examples. In particular, both the closed-form solutions for the discontinuity angles validated by numerical simulations and the corresponding traction-based failure criteria are obtained.

1. Introduction

The onset of macroscopic failure in solids and structures is often signified by highly localized deformations (i.e., strain localization) within bands of small (or even fracture surfaces of negligible) width compared to the length scale of the structure in consideration. Typical examples of the manifestation of strain localization include cracks in concrete, joints in rocks, shear bands in soils, dislocations and slip lines in metals, etc., owing to the overall softening responses of these solids. It is of utmost significance to resolve strain localization and the resulting localized failure while evaluating the residual capacity and preventing the potential catastrophic collapse of structures.

Ever since the pioneering work of Ngo and Scordelis (1967) and Rashid (1968) a large number of different approaches have been developed for the modeling of localized failure in quasi-brittle solids. These approaches range from the classical discrete and smeared crack models (Rots, 1988), to the more advanced strong discontinuity approaches (Hansbo and Hansbo, 2004; Oliver, 1996; Simó et al., 1993; Wells and Sluys, 2001; Wu and Li, 2015; Wu et al., 2015). Restricting the focus to the continuum context, existing formulations can be classified into stress-based (generalized) continuum models or traction-based nonlinear fracture models. In the stress-based family the strain/displacement discontinuities

* Corresponding author. Tel.: +86 20 87112787.
E-mail address: jywu@scut.edu.cn (J.-Y. Wu).

http://dx.doi.org/10.1016/j.ijsolstr.2016.03.005
0020-7683/

upon strain localization are smoothed or smeared. Accordingly, the overall nonlinear behavior of the weakened solid can be described by tensorial constitutive relations in terms of stress *versus* strain equipped with internal variables. Plasticity (Chaboche, 2008; Chen, 1994) and damage mechanics (Krajcinovic, 2003; Lemaitre, 1996) or their combination (Armero and Oller, 2000; Ibrahimbegovic, 2009; Ju, 1989; Ortiz., 1985; Voyiadjis and Dorgan, 2007; Voyiadjis and Kattan, 1992; Wu et al., 2006; Zhu et al., 2010) are frequently employed to develop appropriate inelastic constitutive laws; see Abu Al-Rub and Darabi (2012) and Ibrahimbegovic et al. (2008) and the references therein. To guarantee objectivity of the energy dissipation during the failure process, the softening regime is in general regularized by introducing the fracture energy and an appropriately identified length scale (Bažant and Oh, 1983). Comparatively, in the traction-based approaches strain/displacement jumps are explicitly accounted for by embedding the discontinuities into a solid matrix along preferred orientations. It is in general assumed that energy dissipation is localized into the discontinuities while the bulk remains elastic, between which the traction continuity condition is imposed. Depending on the recoverable/irreversible properties of the discontinuities, vectorial traction-based cohesive zone models of either plastic (Carol et al., 1997), damage (Armero, 1999; Jirásek and Zimmermann, 2001) or combined plastic-damage (Wu, 2011; Wu and Xu, 2011) type can be established. Similarly, the softening law for the discontinuities is also characterized by the fracture energy.

In the traction-based modeling of localized failure in solids, a crucial step is to determine the discontinuity orientation consistently and fix it appropriately, if required. This is a non-trivial task for a new or propagating discontinuity whose orientation is not pre-defined or known *a priori*. For strain or weak discontinuities, the discontinuous bifurcation analysis, pioneered by Hill (1958; 1962), Thomas (1961) and Rice (Borré and Maier, 1989; Rice and Rudnicki, 1980; Rudnicki and Rice, 1975), nowadays becomes the standard tool. Based on the assumption of linear comparison solid (inelastic loading state in both the bulk and localization band) and the traction continuity condition, necessary conditions for the discontinuous bifurcation were identified and the orientation of shear bands can be determined for plastic materials; see the monograph (Lubarda, 2002) and the papers (Jirásek and Rolshoven, 2009; Runesson et al., 1991; Svedberg and Runesson, 1997; Voyiadjis et al., 2005; Vrech and Etse, 2005) among many others. Recently, Sánchez et al. (2008) and Huespe et al. (2009); 2012) successfully applied this strategy to the modeling of ductile fracture in presence of the stress triaxiality (Besson et al., 2003; Remmers et al., 2013).

For strong (displacement) discontinuities, similar arguments were also followed. For instance, Simó et al. (1993) and Oliver (1996) suggested using the discontinuous bifurcation condition together with *null* softening modulus to determine the discontinuity orientation. However, its application to quasi-brittle solids might be questionable, since the actual deformation states upon strain localization, i.e., inelastic loading inside the discontinuity (band) and unloading elastically outside it, are inconsistent with the assumption of linear comparison solids. Consequently, except for some particular cases (e.g., the Rankine and plane strain von Mises models), the strong discontinuity condition (Oliver, 2000; Oliver et al., 1998; 1999) cannot be satisfied in general cases (Oliver et al., 1999). Some kinematic mismatches are observed (Oliver et al., 2012; 2006a) due to mis-prediction of the discontinuity orientation, inevitably resulting in stress locking (Cervera et al., 2012; Mosler, 2005). This fact partially explains the overwhelming popularity of the maximum tensile stress criterion or linear fracture mechanics based ones (Dumstorff and Meschke, 2006) in the numerical modeling of localized failure in brittle and quasi-brittle solids (Wu and Li, 2015; Wu et al., 2015).

Provided the discontinuity orientation is determined, a cohesive zone model is generally introduced to characterize the discontinuity, resulting in either the strong/regularized or embedded/smeared discontinuity models; see Cervera and Wu (2015) for the conformity between these traction-based approaches. However, on the one hand, it is difficult to identify the traction-based failure criterion and involved parameters from available experimental data. On the other hand, the questions whether and when the traction-based cohesive zone model should be introduced cannot be easily identified. Therefore, it would be rather advantageous, if the traction-based failure criterion is derived consistently from a stress-based one and the right instant for introducing the cohesive zone model can be also identified. In this aspect, Oliver and coworkers (Oliver, 2000; Oliver et al., 1998; 1999; 2006a; 2002) made great contributions and derived cohesive zone models by projecting inelastic material laws onto the discontinuity. However, only the classical isotropic damage model (Oliver, 2000; Oliver et al., 2006a; 2002), the Rankine and plane strain von Mises plasticity models (Oliver et al., 1998; 1999) are considered. More general material constitutive laws cannot be sufficiently accounted for as declared in Oliver et al. (1999): "*Obtaining such explicit forms of the discrete constitutive equations is not so straight-forward for other families of elastoplastic models*".

Noticing the above facts, Cervera et al. (2012) proposed directly using the strong discontinuity condition (Oliver, 2000; Oliver et al., 1998; 1999) to determine the discontinuity orientation, so that the stress locking-free property can be guaranteed for a fully softened discontinuity. The discontinuity orientation for von Mises (J_2) plasticity model so obtained were validated by numerical simulations in the cases of plane stress and plane strain. Recently, the authors Wu and Cervera (2013; 2014a, 2014b; 2015) successfully extended this method to a stress-based plastic-damage model with general failure criteria. Not only the discontinuity orientation but also the traction-based cohesive zone model are determined consistently from a given stress-based inelastic material model. Furthermore, the bi-directional connections and in particular, the equivalence conditions, between two complementary methodologies for the modeling of localized failure in quasi-brittle solids, i.e., *traction-based discontinuities localized in an elastic bulk* and *strain localization of a stress-based inelastic softening solid*, have also been established. However, all our previous work assumes implicitly or explicitly that *only relative rigid body motions* occur at both sides of the discontinuity (band) upon strain localization. This restrictive kinematics implies continuous bulk strains across the discontinuity (Wu, 2011). Though the discontinuous bulk strains seldom dominate strain localization in quasi-brittle solids (Oliver et al., 2006b; Wu et al., 2015), the resulting stress continuity might be too restrictive in some cases. Moreover, the aforementioned analyses were mainly intended for the plane stress condition, and the exceptional cases which preclude occurrence of a strong (or regularized) discontinuity were not considered.

The aim of this paper is to make further contributions to the above topics. The novelties are threefold: (*i*) Maxwell's kinematic condition for guaranteeing the occurrence of a strong discontinuity is derived from the traction continuity condition together with the consistent loading/unloading deformation states upon strain localization in quasi-brittle solids; in particular, the assumption of continuous stresses across the discontinuity is disregarded; (*ii*) Closed-form results in both plane stress and plane strain conditions, coincident with those given by numerical simulations (Cervera et al., 2015), are obtained, and the consequences of an additional out-of-plane constraint in the latter case are identified; (*iii*) The aforesaid exceptional case in which the strong discontinuity is precluded for a given stress-based failure criterion is solved by introducing necessary modifications based on the equivalence between

traction- and stress-based approaches established before (Wu and Cervera, 2015). For simplicity only infinitesimal deformations are considered and the possible extension to the finite deformation setting is to be explored later.

This paper is organized as follows. After this introduction, a unified elastoplastic damage framework is presented in Section 2 based on the irreversible thermodynamics with internal variables. Section 3 addresses Maxwell's kinematic constraint upon strain localization in quasi-brittle solids and its application to the above elastoplastic damage model. Closed-form results in 2D conditions of plane stress and plane strain are given in Section 4, together with several classical failure criteria analyzed as illustrative examples. The most relevant conclusions are drawn in Section 5. For the sake of completeness, three appendices are attached to close this paper.

Notation. Compact tensor notation is used in this paper as far as possible. As a general rule, scalars are denoted by italic light-face Greek or Latin letters (e.g. a or λ); vectors and second-order tensors are signified by italic boldface minuscule and majuscule letters like $\boldsymbol{a}$ and $\boldsymbol{A}$, respectively. Fourth-order tensors are identified by blackboard-bold majuscule characters (e.g. $\mathbb{A}$). Symbols $\boldsymbol{I}$ and $\mathbb{I}$ represent the second-order and symmetric fourth-order identity tensors, respectively. Superscripts '$^{\mathrm{T}}$' and '$^{\mathrm{sym}}$' indicate the transposition and symmetrization operations, respectively. The inner products with single and double contractions are denoted by '$\cdot$' and ':', respectively. The dyadic product '$\otimes$' and the symmetrized Kronecker product $\overline{\otimes}$ are defined as

$$\left(\boldsymbol{A}\otimes\boldsymbol{B}\right)_{ijkl}=A_{ij}B_{kl},\qquad \left(\boldsymbol{A}\,\overline{\otimes}\,\boldsymbol{B}\right)_{ijkl}=\frac{1}{2}\left(A_{ik}B_{jl}+A_{il}B_{jk}\right)$$

2. A unified elastoplastic damage framework

Coupled plastic-damage models have been widely adopted to describe stiffness degradation and plastic strains of materials; see Ortiz. (1985), Ju (1989), Voyiadjis and Kattan (1992), Armero and Oller (2000), Ibrahimbegovic et al. (2008) and Zhu et al. (2010) among many others and the large volume of references in the texts (Ibrahimbegovic, 2009; Krajcinovic, 2003). In this section a unified elastoplastic damage framework (Meschke et al., 1998; Wu and Xu, 2011) is presented based on the irreversible thermodynamics with internal variables (Horstemeyer and Bammann, 2010). Both stress- and traction-based elastoplastic damage models can be developed within this framework.

2.1. Stress–strain relations

Confining the discussion to a purely mechanical theory, the second law of thermodynamics (local form) requires that for any admissible deformation process, the energy dissipation rate $\dot{\mathscr{D}}$ has to be non-negative, i.e.,

$$\dot{\mathscr{D}}:=\boldsymbol{\sigma}:\dot{\boldsymbol{\epsilon}}-\dot{\psi}\geq 0 \tag{2.1}$$

where $\boldsymbol{\sigma}$ and $\boldsymbol{\epsilon}$ denote the second-order stress and strain tensors, respectively; $\dot{(\,)}$ represents the rate with respect to the (pseudo-) time; ψ is the Helmholtz free energy density function of the material, which is an important concept for deriving a thermodynamically consistent constitutive model (Lemaitre, 1996).

As usual in the case of isothermal and infinitesimal deformations, it is assumed that the Helmholtz free energy density function ψ admits an uncoupled form (Armero and Oller, 2000; Ju, 1989). To account for both stiffness degradation and irreversible deformations, the free energy density function ψ is postulated as

$$\psi=\psi^{\mathrm{ed}}(\boldsymbol{\epsilon}-\boldsymbol{\epsilon}^{\mathrm{p}},\mathbb{E})+\chi(\kappa) \tag{2.2}$$

where the stored energy function $\psi^{\mathrm{ed}}(\boldsymbol{\epsilon}-\boldsymbol{\epsilon}^{\mathrm{p}},\mathbb{E})$ characterizes the elastic and damage responses of the solid in terms of the recoverable strain tensor $\boldsymbol{\epsilon}-\boldsymbol{\epsilon}^{\mathrm{p}}$ and the variable stiffness tensor $\mathbb{E}$, with $\boldsymbol{\epsilon}^{\mathrm{p}}$ being the irreversible plastic strain tensor; the potential function $\chi(\kappa)$ models the inelastic (damage and plastic) responses in terms of a generic internal variable κ. For the material with linear unloading/reloading responses, the stored strain energy density function $\psi^{\mathrm{ed}}(\cdot,\cdot)$ is expressed as a quadratic form, i.e.,

$$\psi^{\mathrm{ed}}=\frac{1}{2}\left(\boldsymbol{\epsilon}-\boldsymbol{\epsilon}^{\mathrm{p}}\right):\mathbb{E}:\left(\boldsymbol{\epsilon}-\boldsymbol{\epsilon}^{\mathrm{p}}\right) \tag{2.3}$$

Note that the stiffness tensor $\mathbb{E}$ (or, equivalently, the compliance $\mathbb{C}=\mathbb{E}^{-1}$), the plastic strain tensor $\boldsymbol{\epsilon}^{\mathrm{p}}$ and the strain-like variable κ are all internal variables. Therefore, their evolution laws have to be postulated.

Substitution of the definitions (2.2) and (2.3) into the energy dissipation inequality (2.1) yields

$$\begin{aligned}\dot{\mathscr{D}}=&\left[\boldsymbol{\sigma}-\mathbb{E}:\left(\boldsymbol{\epsilon}-\boldsymbol{\epsilon}^{\mathrm{p}}\right)\right]:\left(\dot{\boldsymbol{\epsilon}}-\dot{\boldsymbol{\epsilon}}^{\mathrm{p}}\right)+\boldsymbol{\sigma}:\dot{\boldsymbol{\epsilon}}^{\mathrm{p}}\\&-\frac{1}{2}\left(\boldsymbol{\epsilon}-\boldsymbol{\epsilon}^{\mathrm{p}}\right):\dot{\mathbb{E}}:\left(\boldsymbol{\epsilon}-\boldsymbol{\epsilon}^{\mathrm{p}}\right)-\frac{\partial\chi}{\partial\kappa}\dot{\kappa}\geq 0\end{aligned} \tag{2.4}$$

Calling for the recoverable (arbitrary) property of the elastic and damage strains $\boldsymbol{\epsilon}-\boldsymbol{\epsilon}^{\mathrm{p}}$, it follows that

$$\boldsymbol{\sigma}=\frac{\partial\psi^{\mathrm{ed}}}{\partial\left(\boldsymbol{\epsilon}-\boldsymbol{\epsilon}^{\mathrm{p}}\right)}=\mathbb{E}:\left(\boldsymbol{\epsilon}-\boldsymbol{\epsilon}^{\mathrm{p}}\right),\qquad \boldsymbol{\epsilon}=\mathbb{C}:\boldsymbol{\sigma}+\boldsymbol{\epsilon}^{\mathrm{p}} \tag{2.5}$$

or the rate form

$$\begin{aligned}\dot{\boldsymbol{\sigma}}=&\mathbb{E}:\left(\dot{\boldsymbol{\epsilon}}-\dot{\boldsymbol{\epsilon}}^{\mathrm{p}}\right)+\dot{\mathbb{E}}:\left(\boldsymbol{\epsilon}-\boldsymbol{\epsilon}^{\mathrm{p}}\right)=\mathbb{E}:\left(\dot{\boldsymbol{\epsilon}}-\dot{\boldsymbol{\epsilon}}^{\mathrm{p}}\right)\\&-\mathbb{E}:\dot{\mathbb{C}}:\mathbb{E}:\left(\boldsymbol{\epsilon}-\boldsymbol{\epsilon}^{\mathrm{p}}\right)=\mathbb{E}:\left(\dot{\boldsymbol{\epsilon}}-\dot{\boldsymbol{\epsilon}}^{\mathrm{dis}}\right)\end{aligned} \tag{2.6a}$$

$$\dot{\boldsymbol{\epsilon}}=\mathbb{C}:\dot{\boldsymbol{\sigma}}+\dot{\mathbb{C}}:\boldsymbol{\sigma}+\dot{\boldsymbol{\epsilon}}^{\mathrm{p}}=\mathbb{C}:\dot{\boldsymbol{\sigma}}+\dot{\boldsymbol{\epsilon}}^{\mathrm{dis}} \tag{2.6b}$$

where the relation $\dot{\mathbb{E}}=-\mathbb{E}:\dot{\mathbb{C}}:\mathbb{E}$ resulting from the identity $\mathbb{E}:\mathbb{C}=\mathbb{I}$ has been considered; the *dissipative strain tensor rate* $\dot{\boldsymbol{\epsilon}}^{\mathrm{dis}}$, shown in Fig. 1, consists of the so-called "degradation strain rate" $\dot{\mathbb{C}}:\boldsymbol{\sigma}$ and the plastic one $\dot{\boldsymbol{\epsilon}}^{\mathrm{p}}$

$$\dot{\boldsymbol{\epsilon}}^{\mathrm{dis}}:=\dot{\mathbb{C}}:\boldsymbol{\sigma}+\dot{\boldsymbol{\epsilon}}^{\mathrm{p}} \tag{2.7}$$

As will be clear later from Eq. (2.13), the dissipative strain tensor rate $\dot{\boldsymbol{\epsilon}}^{\mathrm{dis}}$, closely related to the energy dissipation rate $\dot{\mathscr{D}}$, does not correspond to an actual "strain"; it is only defined in rate form when the involved dissipative mechanisms, i.e., damage evolution and plastic flows, are active.

As shown in Fig. 2, the strain tensor $\boldsymbol{\epsilon}$ and the rate $\dot{\boldsymbol{\epsilon}}$ can also be rewritten as the same kinematic decomposition as that in the classical smeared crack model (Armero and Oller, 2000; Rots, 1988)

$$\boldsymbol{\epsilon}=\boldsymbol{\epsilon}^{\mathrm{e}}+\boldsymbol{\epsilon}^{\mathrm{in}}=\mathbb{C}^{0}:\boldsymbol{\sigma}+\boldsymbol{\epsilon}^{\mathrm{in}},\qquad \dot{\boldsymbol{\epsilon}}=\dot{\boldsymbol{\epsilon}}^{\mathrm{e}}+\dot{\boldsymbol{\epsilon}}^{\mathrm{in}}=\mathbb{C}^{0}:\dot{\boldsymbol{\sigma}}+\dot{\boldsymbol{\epsilon}}^{\mathrm{in}} \tag{2.8}$$

Accordingly, the stress $\boldsymbol{\sigma}$ and the rate $\dot{\boldsymbol{\sigma}}$ are given by

$$\boldsymbol{\sigma}=\mathbb{E}^{0}:\boldsymbol{\epsilon}^{\mathrm{e}}=\mathbb{E}^{0}:\left(\boldsymbol{\epsilon}-\boldsymbol{\epsilon}^{\mathrm{in}}\right),\quad \dot{\boldsymbol{\sigma}}=\mathbb{E}^{0}:\dot{\boldsymbol{\epsilon}}^{\mathrm{e}}=\mathbb{E}^{0}:\left(\dot{\boldsymbol{\epsilon}}-\dot{\boldsymbol{\epsilon}}^{\mathrm{in}}\right) \tag{2.9}$$

for the elastic stiffness $\mathbb{E}^{0}$ and compliance $\mathbb{C}^{0}$ of the material, respectively. In the above constitutive relations, the elastic and inelastic strains ($\boldsymbol{\epsilon}^{\mathrm{e}}$, $\boldsymbol{\epsilon}^{\mathrm{in}}$) are expressed as

$$\epsilon^{\mathrm{e}}=\mathbb{C}^{0}:\boldsymbol{\sigma},\qquad \boldsymbol{\epsilon}^{\mathrm{in}}=\boldsymbol{\epsilon}^{\mathrm{d}}+\boldsymbol{\epsilon}^{\mathrm{p}}=\mathbb{C}^{\mathrm{d}}:\boldsymbol{\sigma}+\boldsymbol{\epsilon}^{\mathrm{p}} \tag{2.10}$$

where the damage strain tensor $\epsilon^{\mathrm{d}}:=\mathbb{C}^{\mathrm{d}}:\boldsymbol{\sigma}$ represents the *recoverable* inelastic strain, with $\mathbb{C}^{\mathrm{d}}:=\mathbb{C}-\mathbb{C}^{0}$ being the fourth-order damage compliance which is of identical evolution law as the total one $\mathbb{C}$, i.e., $\dot{\mathbb{C}}^{\mathrm{d}}=\dot{\mathbb{C}}$.

Either of the above two alternative kinematics can be employed to develop elastoplastic damage models. The equivalence between

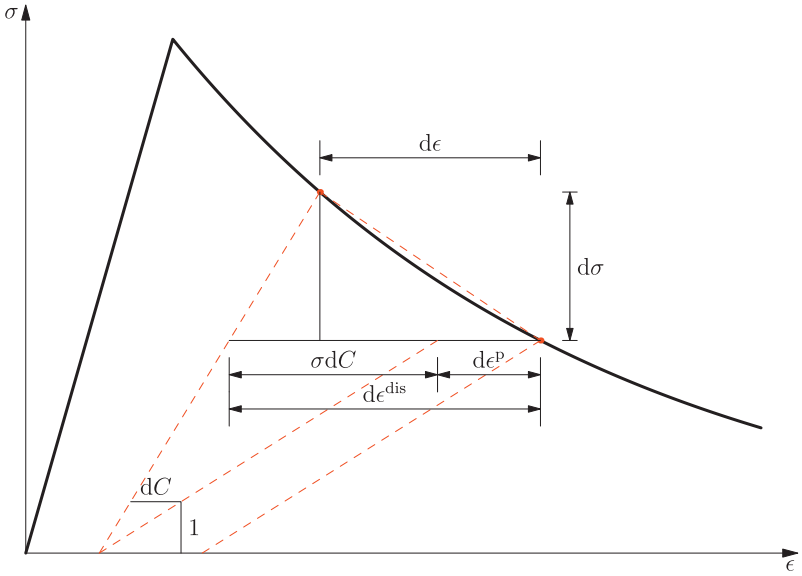

Fig. 1. 1-D definition of the dissipative strain rate tensor and its damage/plastic components.

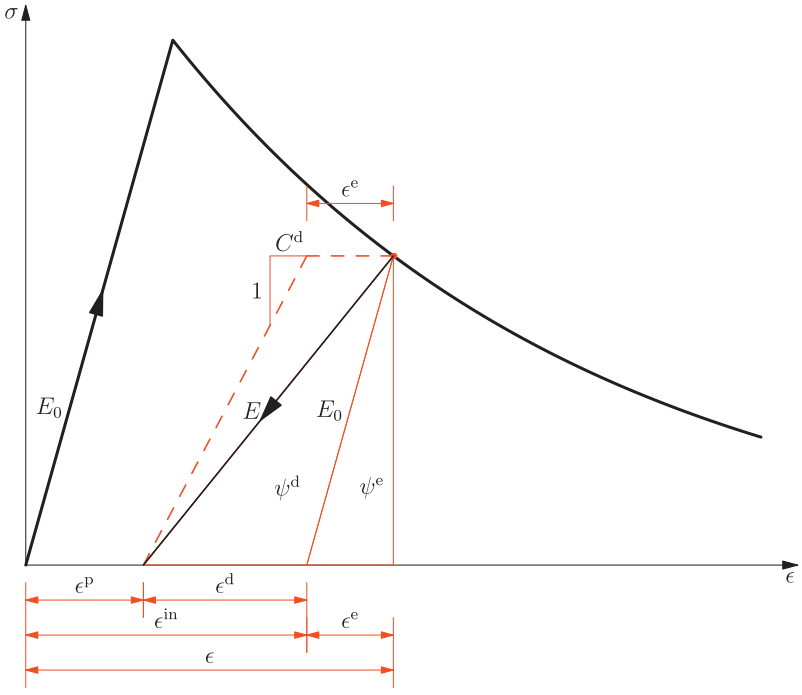

Fig. 2. Different kinematic decompositions adopted in the unified elastoplastic damage model.

the resulting models has been proved recently in Wu and Cervera (2015) and Cervera and Wu (2015).

Remark 2.1. Similarly to the kinematic decomposition (2.8), the stored strain energy density (equal in magnitude to the complementary energy density for the material with linear unloading/reloading behavior) ψ^{ed} defined in Eq. (2.3) can be decomposed as

$$\psi^{\mathrm{ed}} = \frac{1}{2}\,\boldsymbol{\sigma} : \mathbb{C} : \boldsymbol{\sigma} = \psi^{\mathrm{e}} + \psi^{\mathrm{d}} \tag{2.11}$$

where the elastic and damage strain energy densities (also equal in magnitude to their complementary counterparts) (ψ^{e}, ψ^{d}) are given by

$$\psi^{\mathrm{e}} = \frac{1}{2}\,\boldsymbol{\sigma} : \mathbb{C}^0 : \boldsymbol{\sigma} = \frac{1}{2}\,\boldsymbol{\sigma} : \boldsymbol{\epsilon}^{\mathrm{e}} = \frac{1}{2}\,\boldsymbol{\epsilon}^{\mathrm{e}} : \mathbb{E}^0 : \boldsymbol{\epsilon}^{\mathrm{e}} \tag{2.12a}$$

$$\psi^{\mathrm{d}} = \frac{1}{2}\,\boldsymbol{\sigma} : \mathbb{C}^{\mathrm{d}} : \boldsymbol{\sigma} = \frac{1}{2}\,\boldsymbol{\sigma} : \boldsymbol{\epsilon}^{\mathrm{d}} = \frac{1}{2}\,\boldsymbol{\epsilon}^{\mathrm{e}} : \mathbb{E}^0 : \boldsymbol{\epsilon}^{\mathrm{d}} \tag{2.12b}$$

Note again that the damage strain $\boldsymbol{\epsilon}^{\mathrm{d}}$ and the corresponding energy density ψ^{d} are recoverable upon unloading.

2.2. Evolution laws and rate constitutive relations

Besides the above constitutive relations, the energy dissipation inequality (2.4) becomes

$$\dot{\mathscr{D}} = \frac{1}{2}\boldsymbol{\sigma} : \dot{\mathbb{C}} : \boldsymbol{\sigma} + \boldsymbol{\sigma} : \dot{\boldsymbol{\epsilon}}^{\mathrm{p}} - \dot{\chi} = \frac{1}{2}\boldsymbol{\sigma} : \dot{\mathbb{C}} : \boldsymbol{\sigma} + \boldsymbol{\sigma} : \dot{\boldsymbol{\epsilon}}^{\mathrm{p}} + \left(q^0 - q\right)\cdot\dot{\kappa} \geq 0 \tag{2.13}$$

where $q^0 - q := -\partial\chi/\partial\kappa$ denotes the stress-like internal variable conjugate to the strain-like one κ, with q^0 being the initial value of the residual material strength $q(\kappa)$, i.e., $q^0 := q(\kappa = 0)$.

Let us consider a rate-independent softening solid characterized by the failure criterion $\mathcal{F}(\boldsymbol{\sigma}, q) \leq 0$, where the loading function $\mathcal{F}(\boldsymbol{\sigma}, q)$ is a convex, smooth and differentiable homogeneous function of degree $M \geq 1$

$$\mathcal{F}(\boldsymbol{\sigma}, q) = \frac{1}{M}\left(\partial_{\boldsymbol{\sigma}}\mathcal{F} : \boldsymbol{\sigma} + \partial_q\mathcal{F}\cdot q\right) = \frac{1}{M}\left(\boldsymbol{\Lambda} : \boldsymbol{\sigma} - h\cdot q\right) \tag{2.14}$$

for the derivatives $\boldsymbol{\Lambda} := \partial\mathcal{F}/\partial\boldsymbol{\sigma}$ and $h := -\partial\mathcal{F}/\partial q$. As will be shown, either stress- or traction-based loading function $\mathcal{F}(\boldsymbol{\sigma}, q)$ can be employed in the modeling of localized failure in solids.

Accordingly, the postulate of maximum energy dissipation gives the following associated evolution laws (Meschke et al., 1998; Wu and Xu, 2011)

$$\dot{\boldsymbol{\epsilon}}^{\mathrm{dis}} = \dot{\mathbb{C}} : \boldsymbol{\sigma} + \dot{\boldsymbol{\epsilon}}^{\mathrm{p}} = \lambda\boldsymbol{\Lambda}, \qquad \dot{\kappa} = \lambda h \tag{2.15}$$

where the *dissipative flow tensor* $\boldsymbol{\Lambda} := \partial\mathcal{F}/\partial\boldsymbol{\sigma}$ characterizes the dissipative strain rate $\dot{\boldsymbol{\epsilon}}^{\mathrm{dis}}$; the Lagrangian multiplier λ satisfies the classical Kuhn–Tucker loading/unloading conditions

$$\lambda \geq 0, \qquad \mathcal{F}(\boldsymbol{\sigma}, q) \leq 0, \qquad \lambda\mathcal{F}(\boldsymbol{\sigma}, q) = 0 \tag{2.16}$$

Note that the convex loading function (2.14) and the associated evolution laws (2.15) automatically guarantees the energy dissipation inequality (2.13) for any softening law $q(\kappa)$; see Wu and Cervera (2014b).

As a single failure criterion is employed in this work to characterize the inelastic behavior, it is impossible to derive the evolution laws for both the compliance $\mathbb{C}$ and the plastic strain $\boldsymbol{\epsilon}^{\mathrm{p}}$ with no extra assumption. Though other alternatives can be considered, the simplest strategy to overcome this difficulty is to differentiate the damage and plastic contributions to the dissipative strain rate $\dot{\boldsymbol{\epsilon}}^{\mathrm{dis}}$ with a model parameter $\xi \in [0, 1]$. This results in the following relations (Meschke et al., 1998; Ortiz., 1985; Wu and Xu, 2011)

$$\dot{\boldsymbol{\epsilon}}^{\mathrm{p}} = \left(1 - \xi\right)\dot{\boldsymbol{\epsilon}}^{\mathrm{dis}} = \left(1 - \xi\right)\lambda\boldsymbol{\Lambda} \tag{2.17a}$$

$$\dot{\mathbb{C}} : \boldsymbol{\sigma} = \xi\,\dot{\boldsymbol{\epsilon}}^{\mathrm{dis}} = \xi\,\lambda\boldsymbol{\Lambda} \tag{2.17b}$$

For the homogeneous loading function (2.14), the evolution law for the compliance $\mathbb{C}$ satisfying Eq. (2.17b) is given by Meschke et al. (1998); Wu and Xu (2011)

$$\dot{\mathbb{C}} = \dot{\mathbb{C}}^{\mathrm{d}} = \xi\,\lambda\frac{\boldsymbol{\Lambda}\otimes\boldsymbol{\Lambda}}{\boldsymbol{\Lambda} : \boldsymbol{\sigma}} \tag{2.18}$$

The cases $\xi = 0$ and $\xi = 1$ correspond to the classical plasticity model (Chen, 1994) and the elastic damage (degradation) model (Carol et al., 1994; Wu and Xu, 2013), respectively. For the intermediate parameter $\xi \in (0, 1)$, both the material compliance $\mathbb{C}$ (or the damage one $\mathbb{C}^{\mathrm{d}}$) and the plastic strain $\boldsymbol{\epsilon}^{\mathrm{p}}$ are internal variables, resulting in a combined plastic-damage model.

When the material is unloading, i.e., $\mathcal{F}(\boldsymbol{\sigma}, q) < 0$, it follows that $\lambda = 0$; for the loading case, $\lambda > 0$ is solved from the consistency condition $\dot{\mathcal{F}}(\boldsymbol{\sigma}, q) = 0$, i.e.,

$$\dot{\mathcal{F}} = \boldsymbol{\Lambda} : \dot{\boldsymbol{\sigma}} - \lambda h\cdot H\cdot h = \boldsymbol{\Lambda} : \mathbb{E} : \left(\dot{\boldsymbol{\epsilon}} - \lambda\boldsymbol{\Lambda}\right) - \lambda h\cdot H\cdot h = 0 \tag{2.19}$$

or, equivalently,

$$\lambda = \frac{\boldsymbol{\Lambda} : \mathbb{E} : \dot{\boldsymbol{\epsilon}}}{\boldsymbol{\Lambda} : \mathbb{E} : \boldsymbol{\Lambda} + h\cdot H\cdot h} = \frac{\boldsymbol{\Lambda} : \dot{\boldsymbol{\sigma}}}{h\cdot H\cdot h} \tag{2.20}$$

for the softening modulus $H := \partial q/\partial\kappa < 0$. Therefore, the rate constitutive relations are given by

$$\dot{\boldsymbol{\sigma}} = \mathbb{E}_{\mathrm{tan}} : \dot{\boldsymbol{\epsilon}}, \qquad \dot{\boldsymbol{\epsilon}} = \mathbb{C}_{\mathrm{tan}} : \dot{\boldsymbol{\sigma}} \tag{2.21}$$

where the material tangents $\mathbb{E}_{\mathrm{tan}}$ and $\mathbb{C}_{\mathrm{tan}}$ for the loading state (i.e., $\lambda > 0$) are expressed as

$$\mathbb{E}_{\mathrm{tan}} = \mathbb{E} - \frac{\mathbb{E} : \left(\boldsymbol{\Lambda}\otimes\boldsymbol{\Lambda}\right) : \mathbb{E}}{\boldsymbol{\Lambda} : \mathbb{E} : \boldsymbol{\Lambda} + h\cdot H\cdot h} \tag{2.22a}$$

$$\mathbb{C}_{\mathrm{tan}} = \mathbb{C} + \frac{\boldsymbol{\Lambda}\otimes\boldsymbol{\Lambda}}{h\cdot H\cdot h} \tag{2.22b}$$

both being symmetric due to the associated evolution laws considered.

2.3. Fracture energy

For the above elastoplastic-damage model the external energy density supplied to the solid during the failure process, or the so-called specific fracture energy (i.e., energy dissipation per unit volume) g_{f}, can be evaluated as (Wu and Cervera, 2014b; 2015)

$$g_{\mathrm{f}} = \int_0^\infty \boldsymbol{\sigma} : \mathrm{d}\boldsymbol{\epsilon} = \left(1 - \frac{1}{2}\xi\right)\int_0^\infty q(\kappa)\,\mathrm{d}\kappa = \frac{G_{\mathrm{f}}}{b} \tag{2.23}$$

where G_{f} is the fracture energy (i.e., energy dissipation per unit surface area), assumed as a material property; b is a regularization width (see the discussion in next section) where the energy dissipation is lumped. Therefore, the softening law $q(\kappa)$ has to be regularized with respect to the regularization band width b in such a way that the energy dissipation during the whole failure process does not depend on it.

The above regularization procedure was advocated in the crack band theory (Bažant and Oh, 1983). It is equivalent to the cohesive (fictitious) crack model (Barenblatt, 1959; Dugdale, 1960; Hillerborg et al., 1976). In this latter context, Eq. (2.23) is rewritten as

$$G_{\mathrm{f}} = bg_{\mathrm{f}} = \left(1 - \frac{1}{2}\xi\right)\int_0^\infty q(\kappa)b\,\mathrm{d}\kappa = \left(1 - \frac{1}{2}\xi\right)\int_0^\infty q(\tilde{\kappa})\,\mathrm{d}\tilde{\kappa} \tag{2.24}$$

It then allows introducing an equivalent softening law $q(\tilde{\kappa})$ expressed in terms of an alternative *displacement-like* internal variable $\tilde{\kappa}$

$$\tilde{\kappa} := b\kappa, \quad \dot{\tilde{\kappa}} = \tilde{\lambda}h \qquad \Longrightarrow \qquad \tilde{H} = \frac{1}{b}H, \quad \lambda = \frac{1}{b}\tilde{\lambda} \tag{2.25}$$

for the displacement-driven softening modulus $\tilde{H} := \partial q/\partial\tilde{\kappa}$ and the corresponding Lagrangian multiplier $\tilde{\lambda} \geq 0$.

Remark 2.2. It is concluded from Eq. (2.25) that the kinematic internal variables characterizing the inelastic behavior of the material, e.g., the damage compliance $\mathbb{C}^{\mathrm{d}}$, the plastic strain $\boldsymbol{\epsilon}^{\mathrm{p}}$ and the inelastic strain $\boldsymbol{\epsilon}^{\mathrm{in}}$, etc., are all inversely proportional to the band width b.

3. Strain localization analysis

In this section, strain localization in an inelastic solid characterized by the above elastoplastic damage model is analyzed. Compared to the classical discontinuous bifurcation analysis (Hill, 1958; 1962; Rice and Rudnicki, 1980; Rudnicki and Rice, 1975; Runesson et al., 1991; Thomas, 1961), the traction continuity and stress boundedness are guaranteed (Cervera et al., 2012; Wu and Cervera, 2013; 2014a) by reproducing Maxwell's discontinuity kinematics.

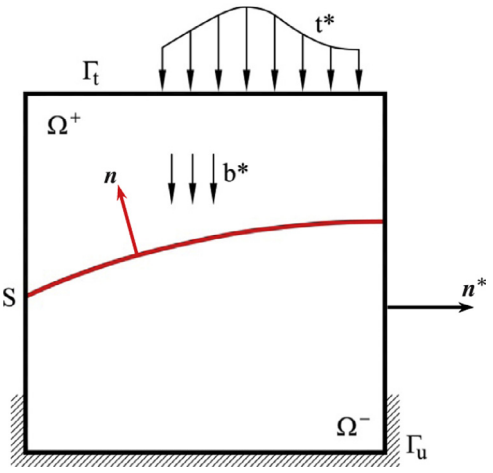

Fig. 3. Problem setting in an elastic solid medium with an internal discontinuity.

More specifically, upon strain localization the dissipative flow tensor characterizing the inelastic evolution laws evolves into a particular structure in terms of a dissipative flow vector and the discontinuity orientation. Accordingly, the tensorial flow components in the directions orthogonal to the discontinuity orientation have to vanish so that the consistent loading/unloading deformation states upon strain localization are correctly represented and a fully stress-free discontinuity (band) can eventually form. This property allows developing a traction-based plastic-damage model for the discontinuity (band). Both the orientation and the traction-based failure criterion can be determined *a posteriori* from the given stress-based counterpart.

3.1. Discontinuity kinematics

Let us consider the domain $\Omega \subset \mathbb{R}^{n_{\text{dim}}}$ $(n_{\text{dim}} = 1, 2, 3)$ shown in Fig. 3. It is occupied by a solid with reference position vector $\boldsymbol{x} \in \mathbb{R}^{n_{\text{dim}}}$. The boundary is denoted by $\Gamma \subset \mathbb{R}^{n_{\text{dim}}-1}$, with an external unit normal vector $\boldsymbol{n}^*$. Deformations of the solid are characterized by the displacement field $\boldsymbol{u} : \Omega \to \mathbb{R}^{n_{\text{dim}}}$ and the infinitesimal strain field $\boldsymbol{\epsilon} := \nabla^{\text{sym}}\boldsymbol{u}$, with $\nabla(\cdot)$ being the spatial gradient operator. The solid is subjected to a distributed body force $\boldsymbol{b}^* : \Omega \to \mathbb{R}^{n_{\text{dim}}}$ per unit volume. Surface tractions $\boldsymbol{t}^* : \Gamma_t \to \mathbb{R}^{n_{\text{dim}}}$ and displacements $\boldsymbol{u}^* : \Gamma_u \to \mathbb{R}^{n_{\text{dim}}}$ are imposed on the disjoint and complementary parts $\Gamma_t \subset \Gamma$ and $\Gamma_u \subset \Gamma$ of the boundary Γ, respectively.

At the early stage of the deformation process, the standard kinematics of a continuum medium apply. In particular, both the displacement and strain fields are continuous and regular (bounded). Upon satisfaction of a specific criterion, strain localization occurs, inevitably inducing strain/displacement jumps. To approximate these jumps, a strong (or regularized) discontinuity may be introduced. In either case, the standard kinematics no longer applies.

Displacement jumps can be described by a strong discontinuity. As depicted in Fig. 4(a), the interface $\mathcal{S}$ splits the solid Ω into two parts Ω^+ and Ω^-, located "ahead of" and "behind" $\mathcal{S}$, respectively, in such a way that $\Omega^+ \cup \Omega^- \cup \mathcal{S} = \Omega$. The discontinuity orientation is characterized by a unit normal vector $\boldsymbol{n}$, pointing from Ω^- to Ω^+ and fixed along time (i.e., $\dot{\boldsymbol{n}} = \boldsymbol{0}$). The strong discontinuity $\mathcal{S}$ causes displacement jumps $\boldsymbol{w} := \boldsymbol{u}(\boldsymbol{x} \in \Omega^+ \cap \mathcal{S}) - \boldsymbol{u}(\boldsymbol{x} \in \Omega^- \cap \mathcal{S})$ across it. In this case, the displacement field $\boldsymbol{u}(\boldsymbol{x})$ is expressed as

$$\boldsymbol{u}(\boldsymbol{x}) = \boldsymbol{u}^-(\boldsymbol{x}) + \mathscr{H}_{\mathcal{S}}(\boldsymbol{x})\,\hat{\boldsymbol{u}}(\boldsymbol{x}), \qquad \hat{\boldsymbol{u}}(\boldsymbol{x}) := \boldsymbol{u}^+(\boldsymbol{x}) - \boldsymbol{u}^-(\boldsymbol{x}) \tag{3.1a}$$

so that the strain field $\boldsymbol{\epsilon}(\boldsymbol{x})$ is given by

$$\boldsymbol{\epsilon}(\boldsymbol{x}) := \nabla^{\text{sym}}\boldsymbol{u}(\boldsymbol{x}) = \nabla^{\text{sym}}\boldsymbol{u}^-(\boldsymbol{x}) + \mathscr{H}_{\mathcal{S}}(\boldsymbol{x})\,\nabla^{\text{sym}}\hat{\boldsymbol{u}}(\boldsymbol{x}) + \big(\boldsymbol{w} \otimes \boldsymbol{n}\big)^{\text{sym}}\,\delta_{\mathcal{S}}(\boldsymbol{x}) \tag{3.1b}$$

where $\boldsymbol{u}^-(\boldsymbol{x})$ and $\boldsymbol{u}^+(\boldsymbol{x})$ denote the displacement fields in the parts Ω^- and Ω^+, respectively, with the former also representing the continuous displacement field in the solid Ω; $\hat{\boldsymbol{u}}(\boldsymbol{x}) : \Omega \to \mathbb{R}^{n_{\text{dim}}}$ signifies the relative displacement field of one part Ω^+ with respect to the other one Ω^-, satisfying the property $\hat{\boldsymbol{u}}(\boldsymbol{x} \in \mathcal{S}) = \boldsymbol{w}$; $\mathscr{H}_{\mathcal{S}}(\boldsymbol{x})$ is the Heaviside function defined at the interface $\mathcal{S}$, i.e., $\mathscr{H}_{\mathcal{S}}(\boldsymbol{x}) = 0$ if $\boldsymbol{x} \in \Omega^- \cup \mathcal{S}$ and $\mathscr{H}_{\mathcal{S}}(\boldsymbol{x}) = 1$ otherwise; $\delta_{\mathcal{S}}(\boldsymbol{x})$ denotes the Dirac-delta at the discontinuity $\mathcal{S}$.

The unbounded strain field (3.1b) resulting from the discontinuous displacement field (3.1a) can be regularized over a discontinuity band $\mathcal{B}$ of finite width b. Note that the width b is not a physical length but a regularization parameter which can be made as small as desired. As shown in Fig. 4(b), the regularized discontinuity (or discontinuity band) $\mathcal{B}$ is delimited by two surfaces $\mathcal{S}^+$ and $\mathcal{S}^-$ parallel to the discontinuity $\mathcal{S}$, i.e., $\Omega^+ \cup \Omega^- \cup \mathcal{B} = \Omega$. In this case, the displacement field $\boldsymbol{u}(\boldsymbol{x})$ is continuous, with an apparent displacement jump $\boldsymbol{w} := \boldsymbol{u}(\boldsymbol{x} \in \Omega^+ \cap \mathcal{S}^+) - \boldsymbol{u}(\boldsymbol{x} \in \Omega^- \cap \mathcal{S}^-)$ across the discontinuity band $\mathcal{B}$. Accordingly, the $\mathcal{C}^0$-continuous displacement field $\boldsymbol{u}(\boldsymbol{x})$ is expressed as (Wu and Li, 2015; Wu et al., 2015)

$$\boldsymbol{u}(\boldsymbol{x}) = \boldsymbol{u}^-(\boldsymbol{x}) + \mathscr{H}_{\mathcal{B}}(\boldsymbol{x})\,\hat{\boldsymbol{u}}(\boldsymbol{x}) \tag{3.2a}$$

and the singular strain field (3.1b) is regularized as

$$\boldsymbol{\epsilon}(\boldsymbol{x}) = \nabla^{\text{sym}}\boldsymbol{u}^-(\boldsymbol{x}) + \mathscr{H}_{\mathcal{B}}(\boldsymbol{x})\,\nabla^{\text{sym}}\hat{\boldsymbol{u}}(\boldsymbol{x}) + \big(\boldsymbol{e} \otimes \boldsymbol{n}\big)^{\text{sym}}\,\Xi_{\mathcal{B}}(\boldsymbol{x}) \tag{3.2b}$$

where the inelastic deformation vector $\boldsymbol{e} := \boldsymbol{w}/b$ is defined as the apparent displacement jump $\boldsymbol{w}$ normalized with respect to the band width b; $\mathscr{H}_{\mathcal{B}}(\boldsymbol{x})$ is a regularized ramp function defined as $\mathscr{H}_{\mathcal{B}}(\boldsymbol{x}) = 0$ if $\boldsymbol{x} \in \Omega^-$, $\mathscr{H}_{\mathcal{B}}(\boldsymbol{x}) = \frac{1}{b}\big(\boldsymbol{x} - \boldsymbol{x}^*\big) \cdot \boldsymbol{n}$ if $\boldsymbol{x} \in \mathcal{B}$, and $\mathscr{H}_{\mathcal{B}}(\boldsymbol{x}) = 1$ otherwise, with $\boldsymbol{x}^*$ being the spatial coordinates of point $\boldsymbol{x}$ projected along the direction $-\boldsymbol{n}$ to the surface $\mathcal{S}^-$; $\Xi_{\mathcal{B}}(\boldsymbol{x})$ denotes the collocation function within the discontinuity band $\mathcal{B}$, i.e., $\Xi_{\mathcal{B}}(\boldsymbol{x}) = 1$ if $\boldsymbol{x} \in \mathcal{B}$ and $\Xi_{\mathcal{B}}(\boldsymbol{x}) = 0$ otherwise.

For either the strong or regularized discontinuity, the strain field $\boldsymbol{\epsilon}(\boldsymbol{x})$ may be discontinuous across it, i.e.,

$$\boldsymbol{\epsilon}_{\mathcal{S}}^+ - \boldsymbol{\epsilon}_{\mathcal{S}}^- = \nabla^{\text{sym}}\hat{\boldsymbol{u}}(\boldsymbol{x} \in \mathcal{S}) \tag{3.3}$$

where $\boldsymbol{\epsilon}_{\mathcal{S}}^+ := \boldsymbol{\epsilon}(\boldsymbol{x} \in \Omega^+ \cap \mathcal{S}^+)$ and $\boldsymbol{\epsilon}_{\mathcal{S}}^- := \boldsymbol{\epsilon}(\boldsymbol{x} \in \Omega^- \cap \mathcal{S}^-)$ represent the strains "ahead of" the surface $\mathcal{S}^+$ and "behind" the surface $\mathcal{S}^-$, respectively. Furthermore, once the discontinuity (band) forms, the strain $\boldsymbol{\epsilon}_{\mathcal{S}} := \boldsymbol{\epsilon}(\boldsymbol{x} \in \mathcal{S})$ at the discontinuity (band) always exhibits a jump with respect to the strain $\boldsymbol{\epsilon}_{\mathcal{S}}^+$ outside it, which verifies Maxwell's compatibility condition

$$[[\boldsymbol{\epsilon}]] := \boldsymbol{\epsilon}_{\mathcal{S}} - \boldsymbol{\epsilon}_{\mathcal{S}}^+ = \big(\boldsymbol{e} \otimes \boldsymbol{n}\big)^{\text{sym}} = \frac{1}{b}\big(\boldsymbol{w} \otimes \boldsymbol{n}\big)^{\text{sym}} \tag{3.4}$$

where the symbol $[[\cdot]] := (\cdot)_{\mathcal{S}} - (\cdot)_{\mathcal{S}}^+$ represents the jump of a specific variable $(\cdot)$. Note that the strain jump $[[\boldsymbol{\epsilon}]]$ is inversely proportional to b for a regularized discontinuity (or unbounded for a strong one).

In summary, the strong discontinuity $\mathcal{S}$ induces a discontinuous displacement field $\boldsymbol{u}(\boldsymbol{x})$ and a singular (unbounded) strain field $\boldsymbol{\epsilon}(\boldsymbol{x})$; see Fig. 5(b). Contrariwise, as shown in Fig. 5(a), the kinematic of a regularized discontinuity is characterized by a continuous displacement field $\boldsymbol{u}(\boldsymbol{x})$ and a regular (bounded) strain field $\boldsymbol{\epsilon}(\boldsymbol{x})$.

Remark 3.1. As the discontinuity band width b tends to zero, it follows that

$$\lim_{b\to 0} \mathscr{H}_{\mathcal{B}}(\boldsymbol{x}) = \mathscr{H}_{\mathcal{S}}(\boldsymbol{x}), \quad \lim_{b\to 0} \frac{1}{b}\Xi_{\mathcal{B}}(\boldsymbol{x}) = \delta_{\mathcal{S}}(\boldsymbol{x}), \quad \lim_{b\to 0} \boldsymbol{e}\,\Xi_{\mathcal{B}}(\boldsymbol{x}) = \boldsymbol{w}\delta_{\mathcal{S}}(\boldsymbol{x}) \tag{3.5}$$

That is, the strong discontinuity can be regarded as the limit of a regularized one, with a vanishing band width $b \to 0$. Reciprocally,

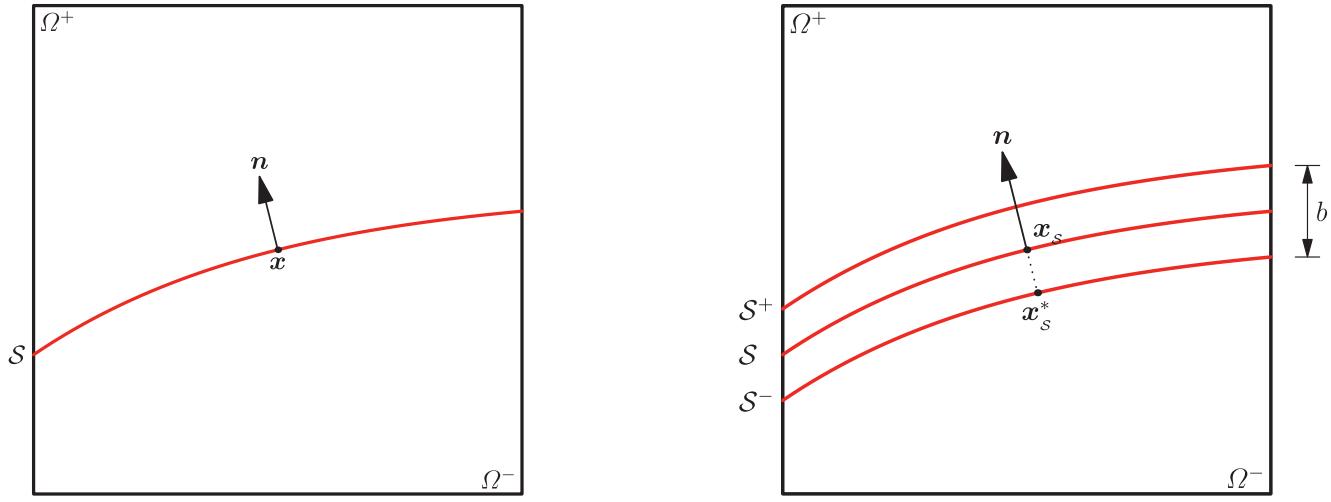

(a) Strong discontinuity (b) Regularized discontinuity

Fig. 4. Strong and regularized discontinuities in a solid.

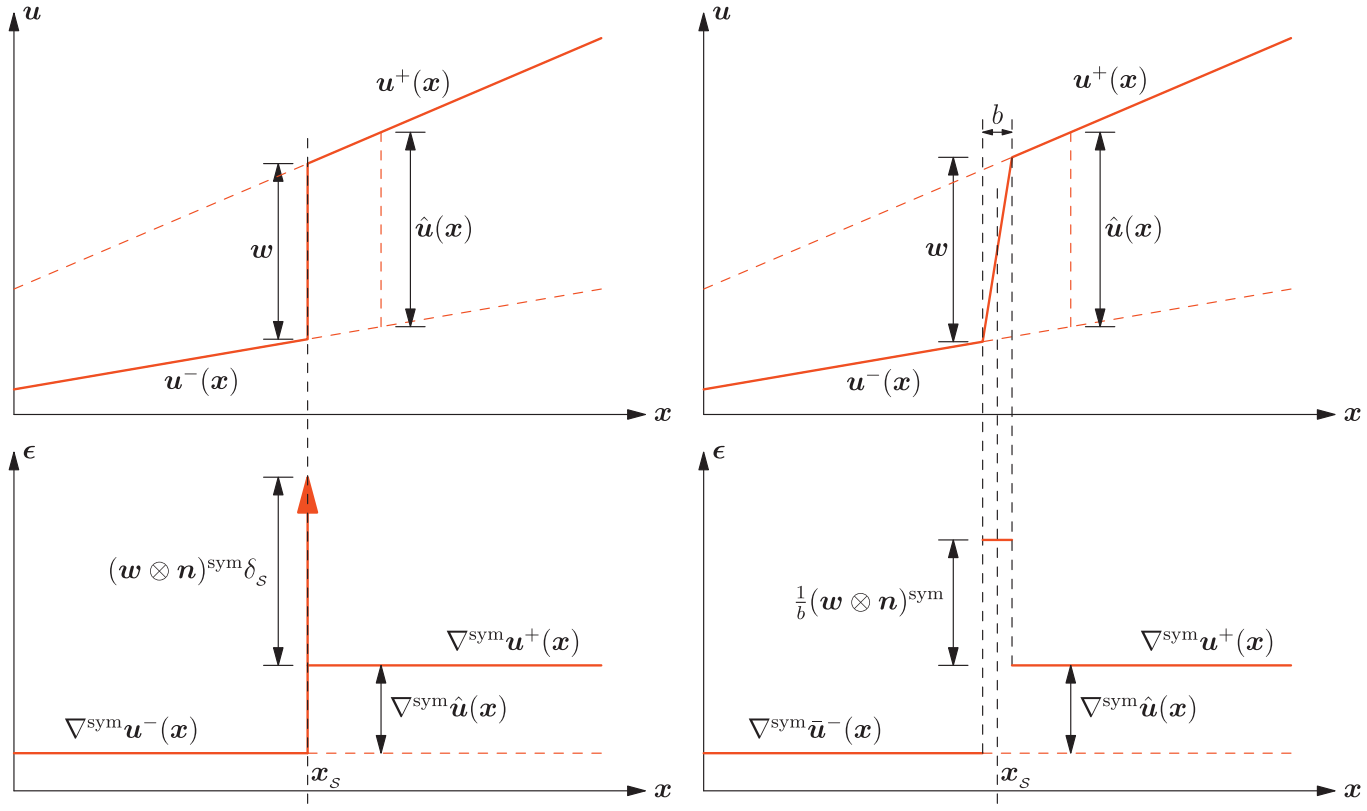

(a) Displacement/strain fields around a strong discontinuity (b) Displacement/strain fields around a regularized discontinuity

Fig. 5. Kinematics of strong/regularized discontinuities.

a discontinuity band can be regarded as the convenient regularization of a strong discontinuity.

Remark 3.2. In our previous work (Cervera and Wu, 2015; Wu and Cervera, 2014b; 2015), it is assumed that the relative displacement field $\hat{\boldsymbol{u}}(\boldsymbol{x})$ is induced only by relative rigid body motions (e.g. translations and rotations) of one part Ω^+ with respect to the other one Ω^- (Wu, 2011). That is, its contribution to the strain field vanishes, i.e., $\nabla^{\text{sym}}\hat{\boldsymbol{u}}(\boldsymbol{x}) = \boldsymbol{0}$ and $\boldsymbol{\epsilon}_s^+ = \boldsymbol{\epsilon}_s^-$. Accordingly, the strains at both sides of the discontinuity are continuous, though the relative displacement field $\hat{\boldsymbol{u}}(\boldsymbol{x})$ is not necessarily constant. This restrictive assumption is disregarded in this work.

3.2. Strain localization of softening solids

For strain localization to occur in a softening solid and to evolve eventually into a fully softened discontinuity at the final stage of the deformation process, material points inside the

discontinuity (band) undergo inelastic loading while those outside it unload elastically (Cervera et al., 2012; Oliver et al., 1999). That is, all the energy dissipative mechanisms (i.e., damage evolution and plastic flows of interest) are restricted to the discontinuity (band) during the subsequent failure process and do not develop in the bulk. Owing to this fact, though the continuous inelastic strains prior to strain localization can be included as in Remark 3.3, they are neglected for the sake of simplicity and only linear elastic bulk materials are considered in this work.

Upon strain localization, the following traction continuity condition has also to be fulfilled in addition to the classical equilibrium equations

$$\boldsymbol{\sigma}_{\mathcal{S}}^{+}\cdot\boldsymbol{n}=\boldsymbol{\sigma}_{\mathcal{S}}^{-}\cdot\boldsymbol{n}=\boldsymbol{t}_{\mathcal{S}} \tag{3.6}$$

where the vector $\boldsymbol{t}_{\mathcal{S}}:=\boldsymbol{\sigma}_{\mathcal{S}}\cdot\boldsymbol{n}$ represents cohesive tractions at the discontinuity; $\boldsymbol{\sigma}_{\mathcal{S}}^{+}:=\boldsymbol{\sigma}(\boldsymbol{x}\in\Omega^{+}\cap\mathcal{S})$, $\boldsymbol{\sigma}_{\mathcal{S}}^{-}:=\boldsymbol{\sigma}(\boldsymbol{x}\in\Omega^{-}\cap\mathcal{S})$ and $\boldsymbol{\sigma}_{\mathcal{S}}:=\boldsymbol{\sigma}(\boldsymbol{x}\in\mathcal{S})$ denote the stresses "ahead of", "behind" and "right" at the discontinuity (band), respectively. In accordance with the generic constitutive relations (2.9), they are determined as

$$\boldsymbol{\sigma}_{\mathcal{S}}^{+}=\mathbb{E}^{0}:\boldsymbol{\epsilon}_{\mathcal{S}}^{+},\qquad \boldsymbol{\sigma}_{\mathcal{S}}^{-}=\mathbb{E}^{0}:\boldsymbol{\epsilon}_{\mathcal{S}}^{-} \tag{3.7a}$$

and

$$\boldsymbol{\sigma}_{\mathcal{S}}=\mathbb{E}^{0}:\left(\boldsymbol{\epsilon}_{\mathcal{S}}-\boldsymbol{\epsilon}_{\mathcal{S}}^{\mathrm{in}}\right) \tag{3.7b}$$

As the bulk strains $\boldsymbol{\epsilon}_{\mathcal{S}}^{+}$ and $\boldsymbol{\epsilon}_{\mathcal{S}}^{-}$ at either side of the discontinuity $\mathcal{S}$ may be discontinuous, the resulting stresses, $\boldsymbol{\sigma}_{\mathcal{S}}^{+}$ and $\boldsymbol{\sigma}_{\mathcal{S}}^{-}$, may also be so.

Let us first consider the continuity between the tractions at both sides of the discontinuity, i.e.,

$$\left(\boldsymbol{\sigma}_{\mathcal{S}}^{+}-\boldsymbol{\sigma}_{\mathcal{S}}^{-}\right)\cdot\boldsymbol{n}=\boldsymbol{n}\cdot\mathbb{E}^{0}:\left(\boldsymbol{\epsilon}_{\mathcal{S}}^{+}-\boldsymbol{\epsilon}_{\mathcal{S}}^{-}\right)=\boldsymbol{0} \tag{3.8}$$

The general expression for the strain difference satisfying Eq. (3.8) is given by (Armero and Kim, 2012; Wu et al., 2015)

$$\boldsymbol{\epsilon}_{\mathcal{S}}^{+}-\boldsymbol{\epsilon}_{\mathcal{S}}^{-}=\alpha_{mm}\boldsymbol{\Lambda}_{mm}+\alpha_{pp}\boldsymbol{\Lambda}_{pp}+\alpha_{mp}\boldsymbol{\Lambda}_{mp} \tag{3.9}$$

where a local orthogonal coordinate system $(\boldsymbol{n},\boldsymbol{m},\boldsymbol{p})$ is introduced at the discontinuity $\mathcal{S}$, with the tangential vectors $\boldsymbol{m}$ and $\boldsymbol{p}$ perpendicular to $\boldsymbol{n}$; the second-order tensors $(\boldsymbol{\Lambda}_{mm},\ \boldsymbol{\Lambda}_{pp},\ \boldsymbol{\Lambda}_{mp})$, with the coefficients $(\alpha_{mm},\ \alpha_{pp},\ \alpha_{mp})$, characterize the in-plane discontinuity modes (two relative stretching ones and a shear one) (Wu et al., 2015)

$$\boldsymbol{\Lambda}_{mm}:=\boldsymbol{m}\otimes\boldsymbol{m}-\nu_{0}\left(\boldsymbol{n}\otimes\boldsymbol{n}+\boldsymbol{p}\otimes\boldsymbol{p}\right) \tag{3.10a}$$

$$\boldsymbol{\Lambda}_{pp}:=\boldsymbol{p}\otimes\boldsymbol{p}-\nu_{0}\left(\boldsymbol{n}\otimes\boldsymbol{n}+\boldsymbol{m}\otimes\boldsymbol{m}\right) \tag{3.10b}$$

$$\boldsymbol{\Lambda}_{mp}:=\left(\boldsymbol{m}\otimes\boldsymbol{p}\right)^{\mathrm{sym}} \tag{3.10c}$$

with ν_0 being Poisson's ratio of the material. Note that the resulting stress field is not necessarily continuous, i.e., $\boldsymbol{\sigma}_{\mathcal{S}}^{+}\neq\boldsymbol{\sigma}_{\mathcal{S}}^{-}$, unless the condition $\alpha_{mm}=\alpha_{pp}=\alpha_{mp}=0$ holds (or, equivalently, the relative displacement field $\hat{\boldsymbol{u}}(\boldsymbol{x})$ is caused only by the rigid body motions of the part Ω^{+} with respect to the other one Ω^{-}). That is, the restrictive stress continuity assumed in our previous work (Wu and Cervera, 2013; 2014a; 2015) is disregarded.

Similarly, the continuity between the tractions across the discontinuity can be expressed as

$$[[\boldsymbol{t}]]:=\left(\boldsymbol{\sigma}_{\mathcal{S}}-\boldsymbol{\sigma}_{\mathcal{S}}^{+}\right)\cdot\boldsymbol{n}=\boldsymbol{n}\cdot\mathbb{E}^{0}:\left[\left(\boldsymbol{e}\otimes\boldsymbol{n}\right)^{\mathrm{sym}}-\boldsymbol{\epsilon}_{\mathcal{S}}^{\mathrm{in}}\right]=\boldsymbol{0} \tag{3.11}$$

It then follows that

$$\left(\boldsymbol{e}\otimes\boldsymbol{n}\right)^{\mathrm{sym}}=\boldsymbol{\epsilon}_{\mathcal{S}}^{\mathrm{in}}+\left(\bar{\alpha}_{mm}\boldsymbol{\Lambda}_{mm}+\bar{\alpha}_{pp}\boldsymbol{\Lambda}_{pp}+\bar{\alpha}_{mp}\boldsymbol{\Lambda}_{mp}\right) \tag{3.12}$$

where the coefficients $(\bar{\alpha}_{mm},\bar{\alpha}_{pp},\bar{\alpha}_{mp})$ are not necessarily coincident with $(\alpha_{mm},\ \alpha_{pp},\ \alpha_{mp})$ in Eq. (3.9).

In the kinematic relation (3.12), on the one hand, the second term of the right hand side is *elastic*, and the coefficients $(\bar{\alpha}_{mm},\bar{\alpha}_{pp},\bar{\alpha}_{mp})$ are all independent of the band width b (otherwise, boundedness of the resulting stress field cannot be guaranteed). On the other hand, the remaining two terms are both inversely proportional to the bandwidth b for the regularized discontinuity (or even singular for the strong one); see Remark 2.2 and Eq. (3.4). Therefore, the kinematic relation (3.12) holds *if and only if the elastic item is canceled*, leading to

$$\boxed{[[\boldsymbol{\epsilon}]]=\boldsymbol{\epsilon}_{\mathcal{S}}^{\mathrm{in}}=\left(\boldsymbol{e}\otimes\boldsymbol{n}\right)^{\mathrm{sym}}=\frac{1}{b}\left(\boldsymbol{w}\otimes\boldsymbol{n}\right)^{\mathrm{sym}}} \tag{3.13}$$

That is, upon strain localization in softening solids, *traction continuity along with stress boundedness* requires that *the strain jump, defined as the difference in the strain fields between the interior/exterior points of the discontinuity (band) and characterized by Maxwell's compatibility condition, has to be completely inelastic*.

Remark 3.3. Inelastic deformations prior to strain localization caused by, e.g., damage and plasticity, can also be incorporated. In this context, the above problem can be regarded as inelastic discontinuities localized in an equivalent elastic medium with a damaged stiffness and some irreversible plastic strains, say $\bar{\mathbb{E}}$ and $\bar{\boldsymbol{\epsilon}}^{\mathrm{p}}$, respectively, which are both frozen once strain localization occurs; see Fig. 6. Namely, one only needs to replace the linear elasticity tensor $\mathbb{E}^0$ by the fixed damaged bulk one $\bar{\mathbb{E}}$, and subtract the fixed bulk plastic strain $\bar{\boldsymbol{\epsilon}}^{\mathrm{p}}$ from the total one, while all the other procedures remain unchanged.

Remark 3.4. Note that the above novel strain localization, and in particular, the kinematic constraint (3.13), can also be written in rate form, but no additional insight in the problem is gained.

3.3. Application to the elastoplastic damage model

For the inelastic strain (2.10) of the elastoplastic damage model, upon strain localization the kinematic condition (3.13) is particularized as

$$\boldsymbol{\epsilon}^{\mathrm{in}}=\left(\boldsymbol{e}\otimes\boldsymbol{n}\right)^{\mathrm{sym}}=\boldsymbol{\epsilon}^{\mathrm{d}}+\boldsymbol{\epsilon}^{\mathrm{p}} \tag{3.14}$$

Recalling the recoverable/irreversible nature of the damage strain $\boldsymbol{\epsilon}^{\mathrm{d}}$ and the plastic one $\boldsymbol{\epsilon}^{\mathrm{p}}$, it follows that (Wu and Cervera, 2014b; 2015)

$$\left(\boldsymbol{e}^{\mathrm{p}}\otimes\boldsymbol{n}\right)^{\mathrm{sym}}=\boldsymbol{\epsilon}^{\mathrm{p}} \tag{3.15a}$$

$$\left(\boldsymbol{e}^{\mathrm{d}}\otimes\boldsymbol{n}\right)^{\mathrm{sym}}=\boldsymbol{\epsilon}^{\mathrm{d}}=\mathbb{C}^{\mathrm{d}}:\boldsymbol{\sigma} \tag{3.15b}$$

where the damage/plastic deformation vectors, $\boldsymbol{e}^{\mathrm{d}}:=\boldsymbol{w}^{\mathrm{d}}/b$ and $\boldsymbol{e}^{\mathrm{p}}:=\boldsymbol{w}^{\mathrm{p}}/b$, are defined as the recoverable and irreversible displacement jumps $(\boldsymbol{w}^{\mathrm{d}},\boldsymbol{w}^{\mathrm{p}})$ normalized with respect to the band width b. Note that the subscript '$_{\mathcal{S}}$' associated with the stress $\boldsymbol{\sigma}_{\mathcal{S}}$ of the discontinuity (band) is dropped here and subsequently for notational simplicity.

Eqs. (2.17a) and (3.15a) imply the existence of a *dissipative flow vector* $\boldsymbol{\gamma}$ satisfying

$$\boxed{\boldsymbol{\Lambda}=\left(\boldsymbol{\gamma}\otimes\boldsymbol{n}\right)^{\mathrm{sym}}} \tag{3.16}$$

or, equivalently (Oliver, 2000),

$$\boldsymbol{\gamma}=2\boldsymbol{n}\cdot\boldsymbol{\Lambda}-\boldsymbol{n}\Lambda_{nn}=\gamma_{n}\boldsymbol{n}+\gamma_{m}\boldsymbol{m}+\gamma_{p}\boldsymbol{p} \tag{3.17}$$

where the components $(\gamma_n,\ \gamma_m,\ \gamma_p)$ of the dissipative flow vector $\boldsymbol{\gamma}$ in the local orthogonal system $(\boldsymbol{n},\boldsymbol{m},\boldsymbol{p})$ are expressed as

$$\gamma_{n}:=\boldsymbol{\gamma}\cdot\boldsymbol{n}=\Lambda_{nn},\quad \gamma_{m}:=\boldsymbol{\gamma}\cdot\boldsymbol{m}=2\Lambda_{nm},\quad \gamma_{p}:=\boldsymbol{\gamma}\cdot\boldsymbol{p}=2\Lambda_{np} \tag{3.18}$$

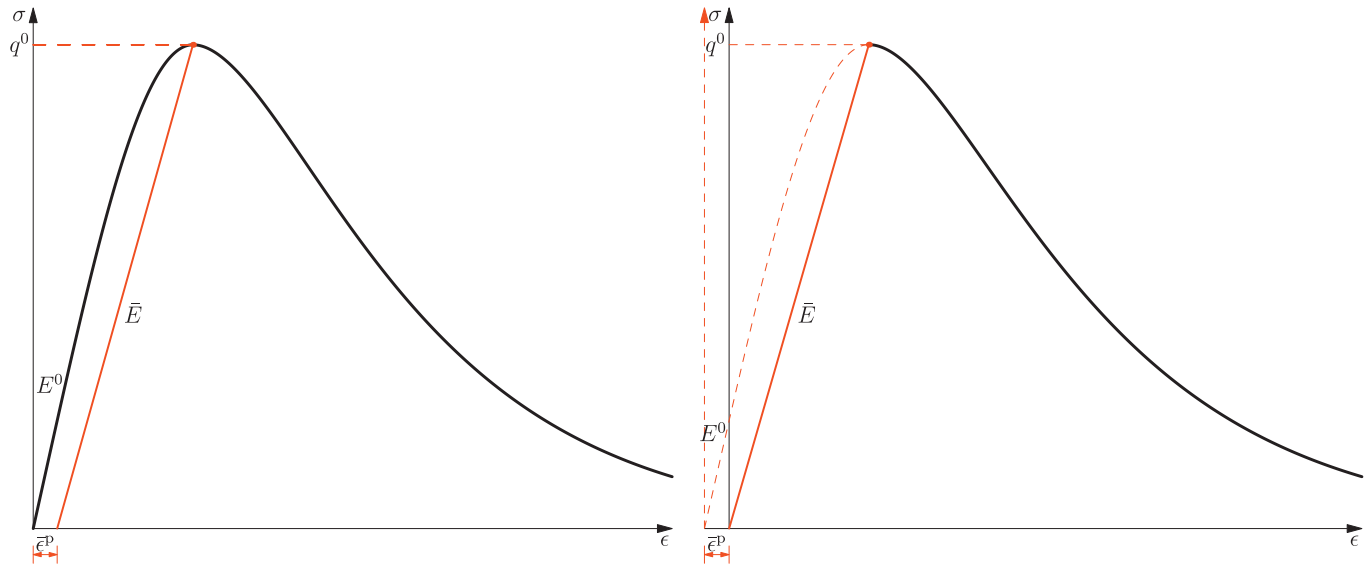

(a) Continuous deformations prior to strain localization (b) Discontinuous deformations post strain localization

Fig. 6. Nonlinear behavior caused by continuous deformations prior to strain localization and the equivalent linear elastic bulk material.

Substitution of the above dissipative flow vector $\boldsymbol{\gamma}$ into the relation (3.16) yields

$$\Lambda_{mm}(\boldsymbol{\theta}^{\rm cr}) = 0, \qquad \Lambda_{pp}(\boldsymbol{\theta}^{\rm cr}) = 0, \qquad \Lambda_{mp}(\boldsymbol{\theta}^{\rm cr}) = 0 \tag{3.19}$$

where $\boldsymbol{\theta}^{\rm cr}$ denote the characteristic discontinuity angles upon which the kinematic constraint (3.16) is satisfied; see Remark 3.5 for general 3D cases. That is, all the dissipative flow components (Λ_{mm}, Λ_{pp}, Λ_{mp}) in the directions normal to the discontinuity (band) have to vanish.

Remark 3.5. To characterize the discontinuity angles $\boldsymbol{\theta}^{\rm cr}$ in general 3D cases, let us first consider the spectral decomposition of the stress $\boldsymbol{\sigma}$ and the coaxial dissipative flow tensor $\boldsymbol{\Lambda} := \partial\mathcal{F}/\partial\boldsymbol{\sigma}$ (Itskov, 2007)

$$\boldsymbol{\sigma} = \sum_{i=1}^{3} \sigma_i \boldsymbol{v}_i \otimes \boldsymbol{v}_i, \qquad \boldsymbol{\Lambda} = \sum_{i=1}^{3} \Lambda_i \boldsymbol{v}_i \otimes \boldsymbol{v}_i \tag{3.20}$$

where σ_i and Λ_i denote the ith principal values, with $\boldsymbol{v}_i$ being the corresponding principal vector. In the coordinate system of principal stresses, the base vectors ($\boldsymbol{n}$, $\boldsymbol{m}$, $\boldsymbol{p}$) can be expressed in terms of a set of characteristic angles $\boldsymbol{\theta} := \{\theta_1, \theta_2, \theta_1, \theta_2\}^{\rm T}$

$$\boldsymbol{n}(\boldsymbol{\theta}) = \left\{ \sin\theta_1 \cos\theta_1,\ \sin\theta_1 \sin\theta_1,\ \cos\theta_1 \right\}^{\rm T} \tag{3.21a}$$

$$\boldsymbol{m}(\boldsymbol{\theta}) = \left\{ \sin\theta_2 \cos\theta_2,\ \sin\theta_2 \sin\theta_2,\ \cos\theta_2 \right\}^{\rm T} \tag{3.21b}$$

$$\boldsymbol{p}(\boldsymbol{\theta}) = \boldsymbol{n}(\boldsymbol{\theta}) \times \boldsymbol{m}(\boldsymbol{\theta}) \tag{3.21c}$$

supplemented with the orthogonal condition

$$C(\boldsymbol{\theta}) := \boldsymbol{n}(\boldsymbol{\theta}) \cdot \boldsymbol{m}(\boldsymbol{\theta}) = \sin\theta_1 \sin\theta_2 \cos\left(\theta_1 - \theta_2\right) + \cos\theta_1 \cos\theta_2 = 0 \tag{3.21d}$$

where (θ_1, θ_2) and (θ_1, θ_2) denote the spherical azimuth and polar angles, respectively; the operator "$\times$" denotes the Gibbs' vector product (the right hand rule is followed). It then follows that

$$\Lambda_{mm}(\boldsymbol{\theta}) = \left(\boldsymbol{m} \otimes \boldsymbol{m}\right) : \boldsymbol{\Lambda}, \quad \Lambda_{pp}(\boldsymbol{\theta}) = \left(\boldsymbol{p} \otimes \boldsymbol{p}\right) : \boldsymbol{\Lambda}, \quad \Lambda_{mp}(\boldsymbol{\theta}) = \left(\boldsymbol{m} \otimes \boldsymbol{p}\right)^{\rm sym} : \boldsymbol{\Lambda} \tag{3.22}$$

With the extra condition (3.21d) handled by the Lagrangian multiplier method, the kinematic constraints (3.19) yield a system of nonlinear equations so that the discontinuity angles $\boldsymbol{\theta}^{\rm cr}$ can be solved.

3.4. Traction-based failure criterion

It follows from the constraints (3.19) that, upon strain localization the failure criterion $\mathcal{F}(\boldsymbol{\sigma}, q) \le 0$ does not depend on the stress components (σ_{mm}, σ_{pp}, σ_{mp}), but is only a function of the tractions $\boldsymbol{t} = \left\{\sigma_{nn}, \sigma_{nm}, \sigma_{np}\right\}^{\rm T}$ acting on the discontinuity (band). Accordingly, provided the characteristic angles $\boldsymbol{\theta}^{\rm cr}$ satisfying the kinematic constraint (3.16) or (3.19) exist, it is always possible to derive a traction-based failure criterion consistent with the given stress-based counterpart $\mathcal{F}(\boldsymbol{\sigma}, q) \le 0$.

Let us consider the following stress-based failure function

$$\mathcal{F}(\boldsymbol{\sigma}, q) := \hat{F}(\mathcal{I}, q) \le 0 \tag{3.23}$$

with the dissipative flow tensor $\boldsymbol{\Lambda}$ given by

$$\boldsymbol{\Lambda} = \hat{\boldsymbol{\Lambda}} := \frac{\partial \hat{F}}{\partial \boldsymbol{\sigma}} = \frac{\partial \hat{F}}{\partial \sigma_1} \boldsymbol{v}_1 \otimes \boldsymbol{v}_1 + \frac{\partial \hat{F}}{\partial I_1} \boldsymbol{I} + \frac{\partial \hat{F}}{\partial J_2} \boldsymbol{s} \tag{3.24}$$

where $\mathcal{I} := \left\{\sigma_1, I_1, J_2\right\}$ collects the invariants of the stress tensor $\boldsymbol{\sigma}$; $\sigma_1 := \boldsymbol{v}_1 \cdot \boldsymbol{\sigma} \cdot \boldsymbol{v}_1$ denotes the major principal stress, with $\boldsymbol{v}_1$ being the corresponding principal vector; $I_1 := \mathrm{tr}(\boldsymbol{\sigma})$ is the first invariant of the stress $\boldsymbol{\sigma}$, and $J_2 := \frac{1}{2}\boldsymbol{s} : \boldsymbol{s}$ represents the second invariant of the deviatoric stress $\boldsymbol{s} := \boldsymbol{\sigma} - \frac{1}{3}\mathrm{tr}(\boldsymbol{\sigma})\boldsymbol{I}$, respectively.

Accordingly, the relation (3.16) becomes

$$\boxed{\left(\boldsymbol{\gamma} \otimes \boldsymbol{n}\right)^{\rm sym} = \boldsymbol{\Lambda}, \qquad \boldsymbol{\Lambda} = \hat{\boldsymbol{\Lambda}} := \frac{\partial \hat{F}}{\partial \boldsymbol{\sigma}}} \tag{3.25}$$

In this case, the orientation $\boldsymbol{n}(\boldsymbol{\theta}^{\rm cr})$ cannot be assumed arbitrarily. But rather, it has to be determined from the kinematic constraints (3.19) for the given stress-based dissipative flow tensor $\boldsymbol{\Lambda} = \hat{\boldsymbol{\Lambda}}$. On the one hand, as the set of equations is nonlinear, the solution may not exist at all. *If and only if* the discontinuity orientation $\boldsymbol{n}(\boldsymbol{\theta}^{\rm cr})$ and the associated dissipative flow vector $\boldsymbol{\gamma}$ satisfying the kinematic constraint (3.25) exist for the given dissipative flow tensor $\hat{\boldsymbol{\Lambda}}$, can the strong (or regularized) discontinuity forms upon strain

localization, and vice versa. On the other hand, provided the solution exists, it depends only on the given failure criterion and the stress state, but not on the elastic properties (i.e., Poisson's ratio ν_0).

Once the discontinuity orientation $\boldsymbol{n}(\boldsymbol{\theta}^{\rm cr})$ is so determined, the corresponding dissipative flow vector $\boldsymbol{\gamma}$ can be obtained from Eqs. (3.17) and (3.18). The projected traction-based failure criterion $f(\boldsymbol{t}, q) \le 0$ is then determined as

$$f(\boldsymbol{t}, q) := \hat{F}(\boldsymbol{\sigma}, q) = \frac{1}{M}\big(\hat{\boldsymbol{\Lambda}} : \boldsymbol{\sigma} - \hat{h} \cdot q\big) = \frac{1}{M}\big(\boldsymbol{\gamma} \cdot \boldsymbol{t} - \hat{h} \cdot q\big) \le 0 \tag{3.26}$$

where the following identity

$$\boldsymbol{\Lambda} : \boldsymbol{\sigma} = \boldsymbol{\gamma} \cdot \big(\boldsymbol{\sigma} \cdot \boldsymbol{n}\big) = \boldsymbol{\gamma} \cdot \boldsymbol{t} \tag{3.27}$$

between the dissipative flow tensor $\boldsymbol{\Lambda}$ and the localized counterpart $\boldsymbol{\gamma}$ has been considered.

Remark 3.6. An alternative strategy is to introduce explicitly the traction-based failure criterion $\hat{f}(\boldsymbol{t}, q) \le 0$, not necessarily coincident with the projected one (3.26), in an *ad hoc* manner. In such approaches (Cervera and Wu, 2015), it is assumed *a priori* that the strong (or regularized) discontinuity can always form once strain localization occurs. Accordingly, the discontinuity orientation cannot be determined uniquely from the kinematic constraints (3.19) for the given traction-based failure criterion $\hat{f}(\boldsymbol{t}, q) \le 0$, unless extra auxiliary conditions are introduced. In our previous work (Cervera and Wu, 2015), the classical Mohr's maximization postulate (Mohr, 1900) is adopted; see Appendix A for its relations to the kinematic constraints (3.19). The bi-directional connections and in particular, the equivalence conditions between these two strategies are referred to in Wu and Cervera (2014b; 2015).

3.5. Localized plastic-damage model

Provided the characteristic angles $\boldsymbol{\theta}^{\rm cr}$ satisfying the kinematic constraint (3.16) exist, the damage evolution law (2.18) becomes

$$\dot{\mathbb{C}} = \dot{\mathbb{C}}^{\rm d} = \big(\dot{\boldsymbol{C}}^{\rm d} \,\overline{\otimes}\, \boldsymbol{N}\big)^{\rm sym} \quad \Longrightarrow \quad \mathbb{C}^{\rm d} = \big(\boldsymbol{C}^{\rm d} \,\overline{\otimes}\, \boldsymbol{N}\big)^{\rm sym} \tag{3.28}$$

for a second-order geometric tensor $\boldsymbol{N} := \boldsymbol{n} \otimes \boldsymbol{n}$. In other words, upon strain localization the material damage behavior is sufficiently characterized by a second-order compliance tensor $\boldsymbol{C}^{\rm d}$ with the following evolution law

$$\dot{\boldsymbol{C}}^{\rm d} = \xi\, \lambda \frac{\boldsymbol{\gamma} \otimes \boldsymbol{\gamma}}{\boldsymbol{\gamma} \cdot \boldsymbol{t}} \tag{3.29}$$

where the identity (3.27) has been considered.

Accordingly, the damage strain tensor (3.15b) is given by

$$\boldsymbol{\epsilon}^{\rm d} = \big(\boldsymbol{e}^{\rm d} \otimes \boldsymbol{n}\big)^{\rm sym} = \Big[\big(\boldsymbol{C}^{\rm d} \cdot \boldsymbol{t}\big) \otimes \boldsymbol{n}\Big]^{\rm sym} \tag{3.30}$$

That is, the discontinuity (band) can be described by the following localized plastic-damage relations

$$\boldsymbol{e}^{\rm d} = \boldsymbol{e} - \boldsymbol{e}^{\rm p} = \boldsymbol{C}^{\rm d} \cdot \boldsymbol{t}, \qquad \boldsymbol{t} = \boldsymbol{E}^{\rm d} \cdot \boldsymbol{e}^{\rm d} = \boldsymbol{E}^{\rm d} \cdot \big(\boldsymbol{e} - \boldsymbol{e}^{\rm p}\big) \tag{3.31a}$$

$$\dot{\boldsymbol{e}}^{\rm p} = \big(1 - \xi\big)\lambda \boldsymbol{\gamma} \tag{3.31b}$$

for the second-order stiffness tensor $\boldsymbol{E}^{\rm d} := \big(\boldsymbol{C}^{\rm d}\big)^{-1}$.

By time differentiation, the rate constitutive relations are expressed as

$$\dot{\boldsymbol{t}} = \boldsymbol{E}^{\rm d} \cdot \big(\dot{\boldsymbol{e}} - \dot{\boldsymbol{e}}^{\rm dis}\big), \qquad \dot{\boldsymbol{e}} = \boldsymbol{C}^{\rm d} \cdot \dot{\boldsymbol{t}} + \dot{\boldsymbol{e}}^{\rm dis} \tag{3.32}$$

where the *dissipative deformation rate* $\dot{\boldsymbol{e}}^{\rm dis}$ is defined as

$$\dot{\boldsymbol{e}}^{\rm dis} := \dot{\boldsymbol{C}}^{\rm d} \cdot \boldsymbol{t} + \dot{\boldsymbol{e}}^{\rm p} = \lambda \boldsymbol{\gamma} \quad \Longrightarrow \quad \big(\dot{\boldsymbol{e}}^{\rm dis} \otimes \boldsymbol{n}\big)^{\rm sym} = \dot{\boldsymbol{\epsilon}}^{\rm dis} = \lambda \boldsymbol{\Lambda} \tag{3.33}$$

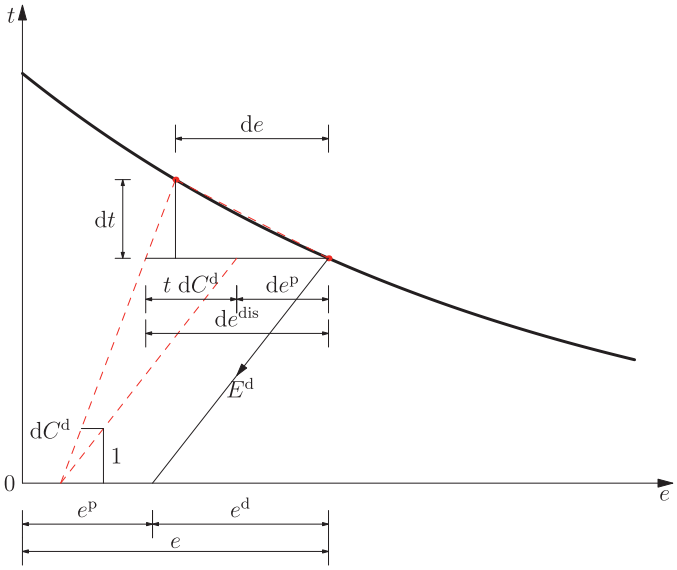

Fig. 7. 1-D definition of the dissipative deformation vector rate and its damage/plastic components.

with $\dot{\boldsymbol{C}}^{\rm d} \cdot \boldsymbol{t}$ and $\dot{\boldsymbol{e}}^{\rm p}$ being its damage and plastic components, respectively; see Fig. 7.

Owing to the relation (3.27), upon strain localization the multiplier $\lambda > 0$ for an active discontinuity band can be determined in terms of the inelastic deformation vector $\boldsymbol{e}$, rather than the strain tensor $\boldsymbol{\epsilon}$ as in Eq. (2.20), i.e.,

$$\lambda = \frac{\boldsymbol{\gamma} \cdot \boldsymbol{E}^{\rm d} \cdot \dot{\boldsymbol{e}}}{\boldsymbol{\gamma} \cdot \boldsymbol{E}^{\rm d} \cdot \boldsymbol{\gamma} + h \cdot H \cdot h} = \frac{\boldsymbol{\gamma} \cdot \dot{\boldsymbol{t}}}{h \cdot H \cdot h} \tag{3.34}$$

It then follows the rate constitutive relations

$$\dot{\boldsymbol{t}} = \boldsymbol{E}^{\rm d} \cdot \big(\dot{\boldsymbol{e}} - \lambda \boldsymbol{\gamma}\big) = \boldsymbol{E}^{\rm d}_{\rm tan} \cdot \dot{\boldsymbol{e}}, \qquad \dot{\boldsymbol{e}} = \boldsymbol{C}^{\rm d} \cdot \dot{\boldsymbol{t}} + \lambda \boldsymbol{\gamma} = \boldsymbol{C}^{\rm d}_{\rm tan} \cdot \dot{\boldsymbol{t}} \tag{3.35}$$

where the tangent stiffness $\boldsymbol{E}^{\rm d}_{\rm tan}$ and compliance $\boldsymbol{C}^{\rm d}_{\rm tan}$ are expressed as

$$\boldsymbol{E}^{\rm d}_{\rm tan} = \boldsymbol{E}^{\rm d} - \frac{\boldsymbol{E}^{\rm d} \cdot \big(\boldsymbol{\gamma} \otimes \boldsymbol{\gamma}\big) \cdot \boldsymbol{E}^{\rm d}}{\boldsymbol{\gamma} \cdot \boldsymbol{E}^{\rm d} \cdot \boldsymbol{\gamma} + h \cdot H \cdot h} \tag{3.36a}$$

$$\boldsymbol{C}^{\rm d}_{\rm tan} = \boldsymbol{C}^{\rm d} + \frac{\boldsymbol{\gamma} \otimes \boldsymbol{\gamma}}{h \cdot H \cdot h} \tag{3.36b}$$

for the active discontinuity (band).

Therefore, provided the kinematic constraint resulting from the traction continuity along with stress boundedness is fulfilled, consistent traction-based constitutive laws for the discontinuity (band) naturally emerge from the strain localization analysis of stress-based models with regularized softening regime.

Remark 3.7. For the damage compliance tensor $\mathbb{C}^{\rm d}$ in Eq. $(3.28)_2$, the (complementary) damage free energy density function $\psi^{\rm d}$ introduced in Eq. (2.12b) is lumped within the discontinuity (band), i.e.,

$$\psi^{\rm d} = \frac{1}{2}\boldsymbol{\sigma} : \mathbb{C}^{\rm d} : \boldsymbol{\sigma} = \frac{1}{2}\boldsymbol{t} \cdot \boldsymbol{C}^{\rm d} \cdot \boldsymbol{t} = \frac{1}{2}\boldsymbol{e}^{\rm d} \cdot \boldsymbol{E}^{\rm d} \cdot \boldsymbol{e}^{\rm d} \tag{3.37}$$

Similarly, the energy dissipation rate (2.13) becomes

$$\dot{\mathscr{D}} = \frac{1}{2}\,\boldsymbol{t} \cdot \dot{\boldsymbol{C}}^{\rm d} \cdot \boldsymbol{t} + \boldsymbol{t} \cdot \dot{\boldsymbol{e}}^{\rm p} + \big(q^0 - q\big) \cdot \dot{\kappa} \ge 0 \tag{3.38}$$

Accordingly, the above localized plastic-damage model can also be derived by an alternative derivation (Wu and Cervera, 2014b).

Remark 3.8. In the above localized plastic-damage model, the *strain-like* internal variable κ is employed in the softening law $q(\kappa)$.

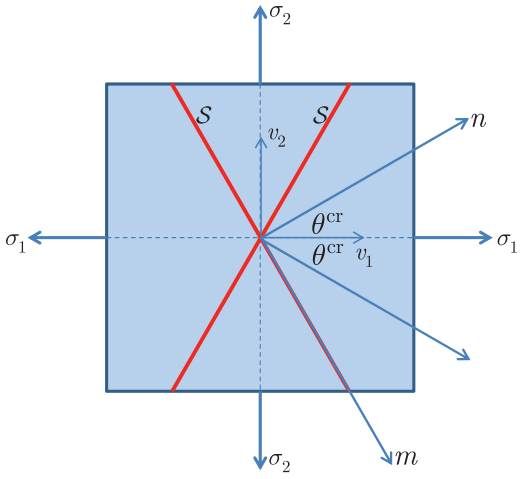

Fig. 8. Definition of the discontinuity angle.

Accordingly, the resulting localized constitutive laws are expressed in terms of the traction $\boldsymbol{t}$ and the inelastic deformation vector $\boldsymbol{e}$. Recalling the relations (2.25), the equivalent localized model in terms of tractions $\boldsymbol{t}$ *versus* displacement jumps $\boldsymbol{w}$ can also be developed. The details are omitted here.

4. Plane stress and plane strain cases

In this section let us consider strain localization of a 2D softening solid $\Omega \subset \mathbb{R}^2$ in plane stress and plane strain shown in Fig. 8. The in-plane principal stresses are denoted by σ_1 and σ_2 ($\sigma_1 \geq \sigma_2$), respectively, while the third one σ_3 is orthogonal to that plane. In such 2D cases the discontinuity orientation can be characterized by the inclination angle (counterclockwise) $\theta \in [-\pi/2, \pi/2]$ between the normal vector $\boldsymbol{n}$ and the principal vector $\boldsymbol{v}_1$ of the stress tensor. The tangential vectors $\boldsymbol{m}$ and $\boldsymbol{p}$ of the discontinuity $\mathcal{S}$ are located on and perpendicular to the plane of interest, respectively. The task is to derive explicitly the discontinuity angle $\theta^{\rm cr}$ and the traction-based failure criterion $f(\boldsymbol{t}, q) \leq 0$ from the given stress-based one $\hat{F}(\boldsymbol{\sigma}, q) \leq 0$. Several classical failure criteria, i.e., Rankine, Mohr–Coulomb, von Mises and Drucker–Prager models, are considered; see Wu and Cervera (2014b) for more general examples.

4.1. Discontinuity angle

For a given stress-based failure criterion $\hat{F}(\boldsymbol{\sigma}, q) \leq 0$, the discontinuity angle $\theta^{\rm cr}$ can be determined explicitly through the projection relation (3.25) or more specifically, through the kinematic constraints (3.19), i.e.,

$$\hat{\Lambda}_{mm}(\theta^{\rm cr}) = 0, \qquad \hat{\Lambda}_{pp}(\theta^{\rm cr}) = 0 \tag{4.1}$$

Note that in 2D cases the other constraint $\hat{\Lambda}_{mp}(\theta^{\rm cr}) = 0$ is automatically satisfied.

It follows from the Mohr's circle and the constraint $\hat{\Lambda}_{mm}(\theta^{\rm cr}) = 0$ that (Wu and Cervera, 2014b; 2015)

$$\sin^2\theta^{\rm cr} = -\frac{\hat{\Lambda}_2}{\hat{\Lambda}_1 - \hat{\Lambda}_2}, \qquad \cos^2\theta^{\rm cr} = \frac{\hat{\Lambda}_1}{\hat{\Lambda}_1 - \hat{\Lambda}_2} \tag{4.2}$$

where $\hat{\Lambda}_1$ and $\hat{\Lambda}_2$ (assuming $\hat{\Lambda}_1 \geq \hat{\Lambda}_2$ as usual) denote the principal values of the dissipative flow tensor $\boldsymbol{\Lambda}$. Note that the above results apply upon the conditions $\hat{\Lambda}_1 \geq 0$ and $\hat{\Lambda}_2 \leq 0$; see Appendix B for the exceptional cases.

Obviously, the discontinuity angle $\theta^{\rm cr}$ depends on the ratio $\hat{\Lambda}_2/\hat{\Lambda}_1$ or the stress state upon strain localization. In particular, the states of plane stress and plane strain have to be discriminated regarding the remaining condition, $\hat{\Lambda}_{pp} = 0$.

4.1.1. Plane stress

In the case of plane stress, the component $\sigma_{pp} = \sigma_3 = 0$ vanishes so that it is not necessary to consider the vanishing dissipative flow component $\hat{\Lambda}_{pp} = \hat{\Lambda}_3 = 0$. Therefore, once the initial failure surface is reached, i.e., $\hat{F}(\boldsymbol{\sigma}, q^0) = 0$, the strong (or regularized) discontinuity forms at the same instant, with the orientation determined from Eq. (4.2).

4.1.2. Plane strain

In the case of plane strain (i.e. $\epsilon_3 = 0$), on the one hand, the elastic out-of-plane stress σ_3 is given by

$$\sigma_3 = \nu_0\big(\sigma_1 + \sigma_2\big) \tag{4.3}$$

On the other hand, for the homogeneous loading function $\hat{F}(\boldsymbol{\sigma}, q)$ of degree $M \leq 2$, the condition $\hat{\Lambda}_{pp} = 0$ gives

$$\hat{\Lambda}_{pp} = \hat{\Lambda}_3 = 0 \qquad \Longrightarrow \qquad \sigma_3 = \eta_1\big(\sigma_1 + \sigma_2\big) + \eta_2 q \tag{4.4}$$

where η_1 and η_2 are related to the model parameters involved in the specified stress-based failure criterion $\hat{F}(\boldsymbol{\sigma}, q) \leq 0$; see the examples presented later. As the in-plane principal values $\hat{\Lambda}_1$ and $\hat{\Lambda}_2$ depend on the out-of-plane stress $\sigma_3 \neq 0$, the discontinuity angle $\theta^{\rm cr}$, still determined from Eq. (4.2), is affected by this extra plane strain localization condition.

The out-of-plane stress (4.4), necessary for plane strain localization, is in general different from the elastic value (4.3). Furthermore, the initial limit surface $\hat{F}(\boldsymbol{\sigma}, q^0) = 0$ will be reached earlier with the elastic out-of-plane stress (4.3) than with the localized one (4.4). Accordingly, except for very particular cases, strain localization cannot occur at the onset of softening. Rather, some (continuous) inelastic deformations and substantial rotation of the principal strain directions have to occur at the beginning of the softening regime, until the plane strain localization condition (4.4) is fulfilled. From that moment on, the (continuous) inelastic deformations in the bulk material are frozen (unloading), and the discontinuous inelastic deformations within the discontinuity (band) continue growing due to strain localization. That is, the bulk material is considered as linear elastic after strain localization occurs, however, with degraded (unloading) stiffness and plastic deformations corresponding to those at the time when strain localization is initiated. The above delayed strain localization in the plane strain condition, similarly to the transited continuous–discontinuous failure (Jirásek and Zimmermann, 2001) illustrated in Fig. 9, was numerically observed in Cervera et al. (2012) for von Mises (J_2) model. As shown in Section 4.6, it also occurs for other failure criteria like the classical Drucker–Prager model.

Remark 4.1. In the case of plane stress, the discontinuity angle $\theta^{\rm cr}$ determined from Eq. (4.2) coincides with that obtained from the classical discontinuous bifurcation analysis (Runesson et al., 1991) for the material model with associated evolution laws. Comparatively, in the plane strain state the discontinuous bifurcation analysis gives (Runesson et al., 1991)

$$\sin^2\theta^{\rm cr} = -\frac{\hat{\Lambda}_2 + \nu_0\hat{\Lambda}_3}{\hat{\Lambda}_1 - \hat{\Lambda}_2}, \qquad \cos^2\theta^{\rm cr} = \frac{\hat{\Lambda}_1 + \nu_0\hat{\Lambda}_3}{\hat{\Lambda}_1 - \hat{\Lambda}_2} \tag{4.5}$$

The above results coincide with Eq. (4.2) if $\nu_0 = 0$ or $\hat{\Lambda}_3 = 0$. The later condition, $\hat{\Lambda}_3 = 0$, necessary for the strong or regularized discontinuity to form and to develop eventually into a fully softened one, is not accounted for in the classical discontinuous bifurcation analysis. An exception is the so-called zero-extension line theory for Mohr–Coulomb materials; see Ottosen and Runesson (1991); Roscoe (1970) for the details. Therefore, the results derived from Maxwell's compatibility condition are consistent with, but more demanding than, the classical ones.

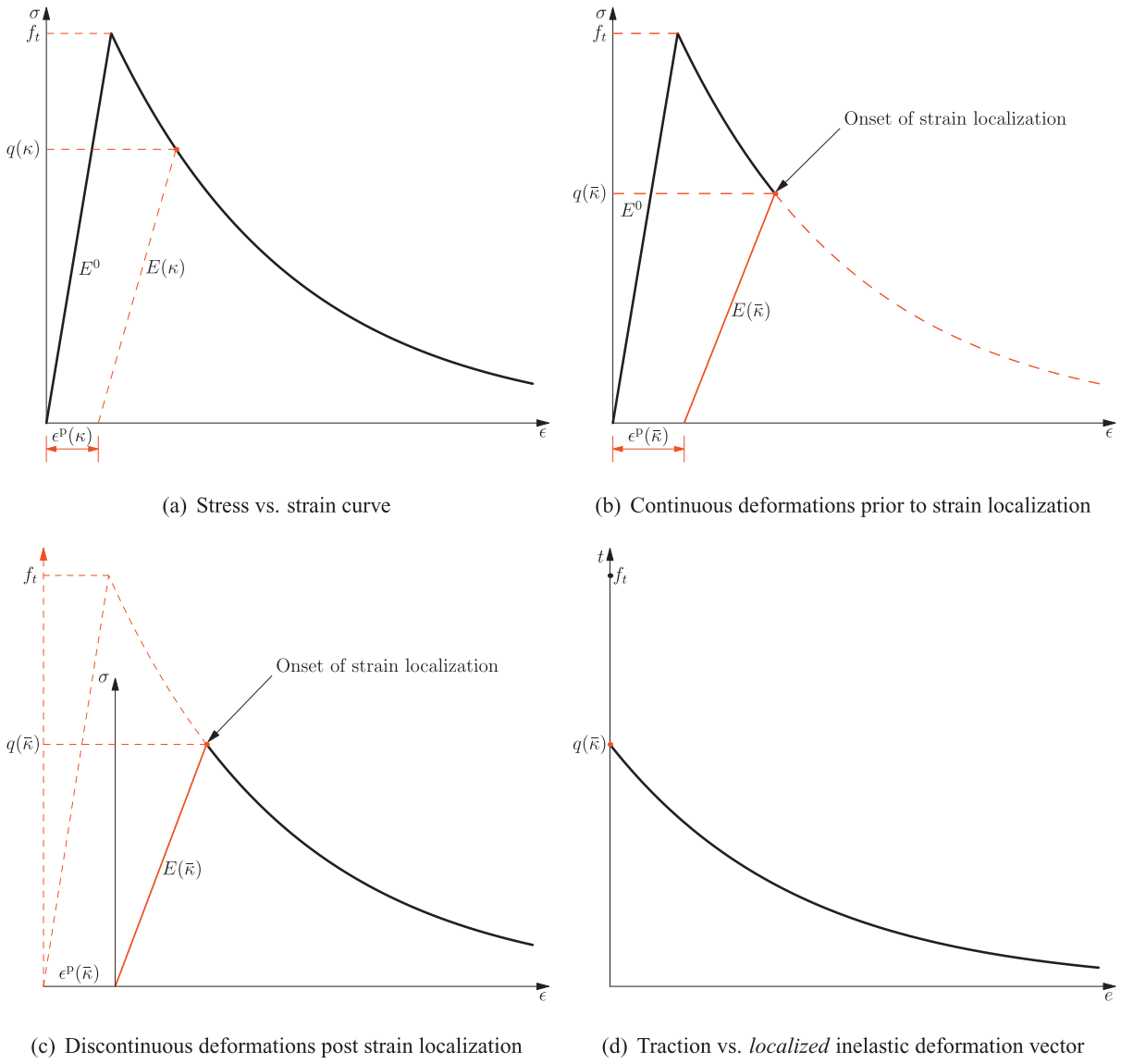

(a) Stress vs. strain curve

(b) Continuous deformations prior to strain localization

(c) Discontinuous deformations post strain localization

(d) Traction vs. *localized* inelastic deformation vector

Fig. 9. Delayed strain localization in the condition of plane strain. Here, κ denotes the strain-like internal variable, and $\bar{\kappa}$ represents the corresponding value at the onset of strain localization.

4.2. Traction-based failure criterion

With the discontinuity angle θ^{cr} determined from Eq. (4.2), the normal and tangential components (γ_n, γ_m) of the dissipative flow vector $\boldsymbol{\gamma}$ are given by

$$\gamma_n = \hat{\Lambda}_{nn}(\theta^{\mathrm{cr}}) = \left(\hat{\Lambda}_1 - \hat{\Lambda}_2\right)\cos(2\theta^{\mathrm{cr}}) = \hat{\Lambda}_1 + \hat{\Lambda}_2 \tag{4.6a}$$

$$\gamma_m = 2\hat{\Lambda}_{nm}(\theta^{\mathrm{cr}}) = \left(\hat{\Lambda}_1 - \hat{\Lambda}_2\right)\sin(2\theta^{\mathrm{cr}}) = 2\,\mathrm{sign}(\sigma_{nm})\sqrt{-\hat{\Lambda}_1\hat{\Lambda}_2} \tag{4.6b}$$

for the sign function $\mathrm{sign}(\cdot)$.

In accordance with Eq. (3.26), the stress-based failure criterion $\hat{F}(\boldsymbol{\sigma}, q) \le 0$ is projected to the orientation $\boldsymbol{n}(\theta^{\mathrm{cr}})$, leading to the following traction-based counterpart

$$f(\boldsymbol{t}, q) = \frac{1}{M}\left[\left(\hat{\Lambda}_1 + \hat{\Lambda}_2\right)t_n + 2\sqrt{-\hat{\Lambda}_1\hat{\Lambda}_2}\,\left|t_m\right| - \hat{h}\cdot q\right] \le 0 \tag{4.7}$$

Similarly, the projected traction-based failure criterion (4.7) holds for the cases $\hat{\Lambda}_1 \ge 0$ and $\hat{\Lambda}_2 \le 0$; the exceptional cases are also dealt with in Appendix B.

Remark 4.2. For the projected traction-based failure criterion (4.7), it follows that

$$\frac{\partial f}{\partial \theta} = -\frac{1}{2}(\sigma_1 - \sigma_2)\left[\left(\hat{\Lambda}_1 + \hat{\Lambda}_2\right) - \left(\hat{\Lambda}_1 - \hat{\Lambda}_2\right)\cos(2\theta)\right]\sin(2\theta) \tag{4.8a}$$

$$\frac{\partial^2 f}{\partial \theta^2} = -(\sigma_1 - \sigma_2)\left[\left(\hat{\Lambda}_1 + \hat{\Lambda}_2\right)\cos(2\theta) - \left(\hat{\Lambda}_1 - \hat{\Lambda}_2\right)\cos(4\theta)\right] \tag{4.8b}$$

It can be verified for the discontinuity angle θ^{cr} given from Eq. (4.2) that

$$\left.\frac{\partial f}{\partial \theta}\right|_{\theta^{\mathrm{cr}}} = 0, \qquad \left.\frac{\partial^2 f}{\partial \theta^2}\right|_{\theta^{\mathrm{cr}}} < 0 \tag{4.9}$$

Therefore, provided strain localization occurs, the tractions (t_n, t_m) do maximize the projected traction-based failure criterion $f(\boldsymbol{t}, q) \le 0$ as in Mohr's maximization postulate.

4.3. Example: Rankine criterion

The Rankine criterion, widely adopted for the modeling of tensile failure in quasi-brittle materials, is expressed in terms of the major principal stress $\sigma_1 = \boldsymbol{v}_1 \cdot \boldsymbol{\sigma} \cdot \boldsymbol{v}_1 > 0$ as

$$\hat{F}(\boldsymbol{\sigma}, q) = \langle \sigma_1 \rangle - q = \mathscr{H}(\sigma_1)\, \sigma_1 - q \le 0 \tag{4.10}$$

where the Macaulay brackets $\langle \cdot \rangle$ is defined as $\langle x \rangle = \max(x, 0)$.

In both plane stress and plane strain conditions, it follows from Eq. (4.2) that

$$\sin^2\theta^{\rm cr} = 0 \qquad \Longrightarrow \qquad \theta^{\rm cr} = 0 \tag{4.11}$$

As expected, only a mode I discontinuity (in the context of fracture mechanics) can be initiated. Furthermore, with the discontinuity angle (4.11), the traction-based failure criterion (4.7) becomes

$$f(\boldsymbol{t}, q) = \langle t_n \rangle - q \le 0 \tag{4.12}$$

where the relation $\sigma_1 = \boldsymbol{n} \cdot \boldsymbol{\sigma} \cdot \boldsymbol{n} = t_n$ has been considered for mode-I failure.

4.4. Example: Mohr–Coulomb criterion

Let us then consider the Mohr–Coulomb criterion, with the following failure function

$$\hat{F}(\boldsymbol{\sigma}, q) = \begin{cases} \frac{1}{2}\Big[(\sigma_1+\sigma_3)\sin\varphi + (\sigma_1-\sigma_3)\Big] - q\cos\varphi & \text{Region 1}: \sigma_1 \ge \sigma_2 \ge \sigma_3 \\ \frac{1}{2}\Big[(\sigma_1+\sigma_2)\sin\varphi + (\sigma_1-\sigma_2)\Big] - q\cos\varphi & \text{Region 2}: \sigma_1 \ge \sigma_3 \ge \sigma_2 \\ \frac{1}{2}\Big[(\sigma_3+\sigma_2)\sin\varphi + (\sigma_3-\sigma_2)\Big] - q\cos\varphi & \text{Region 3}: \sigma_3 \ge \sigma_1 \ge \sigma_2 \end{cases} \tag{4.13}$$

where the internal friction angle $\varphi \in [0, \pi/2]$ is

$$\sin\varphi = \frac{\rho - 1}{\rho + 1} \qquad \Longleftrightarrow \qquad \rho = \frac{1+\sin\varphi}{1-\sin\varphi} \tag{4.14}$$

for the ratio $\rho := f_c/f_t \ge 1$ between the uniaxial compressive strength f_c and the tensile one f_t.

In the case of plane stress ($\sigma_3 = 0$), it follows from Eq. (4.2) that $\theta^{\rm cr} = 0$ in Region 1 and $\theta^{\rm cr} = \pi/2$ in Region 3, respectively; in Region 2 (i.e., $\sigma_1 \ge \sigma_3 \ge \sigma_2$), the discontinuity angle $\theta^{\rm cr}$ is determined as

$$\sin^2\theta^{\rm cr} = \frac{1}{2}(1 - \sin\varphi) \qquad \Longrightarrow \qquad \theta^{\rm cr} = \pm\left(\frac{\pi}{4} - \frac{\varphi}{2}\right) \tag{4.15}$$

The above results coincide with those obtained from Mohr's maximization postulate.

In the case of plane strain, the extra constraint $\hat{\Lambda}_3 = 0$ cannot be satisfied in Regions 1 and 3; only in Region 2 (i.e., $\sigma_1 \ge \sigma_3 \ge \sigma_2$) can strain localization occur, with the same discontinuity angle (4.15).

For the discontinuity angle (4.15), in Region 2 ($\sigma_1 \ge \sigma_3 \ge \sigma_2$) the traction-based failure criterion (4.6) reads

$$f(\boldsymbol{t}, q) = \cos\varphi\Big(t_n \tan\varphi + \big|t_m\big| - q\Big) \le 0 \tag{4.16a}$$

or, equivalently,

$$\tan\varphi \cdot t_n + \big|t_m\big| - q \le 0 \tag{4.16b}$$

in both cases of plane stress and plane strain. This is exactly the classical traction-based Mohr–Coulomb criterion.

Remark 4.3. Tresca's criterion is recovered for the friction angle $\varphi = 0$ in the Mohr–Coulomb criterion (4.13). In Region 2 ($\sigma_1 \ge \sigma_3 \ge \sigma_2$), the discontinuity angle is then $\theta^{\rm cr} = \pi/4$ so that

$$f(\boldsymbol{t}, q) = \big|t_m\big| - q \le 0 \tag{4.17}$$

for both cases of plane stress and plane strain.

4.5. Example: von Mises (J_2) criterion

The von Mises (J_2) criterion is now considered

$$\hat{F}(\boldsymbol{\sigma}, q) = \sqrt{3J_2} - q = \sqrt{\frac{3}{2}}\,\big\|\boldsymbol{s}\big\| - q \le 0 \tag{4.18}$$

in terms of the second invariant $J_2 := \frac{1}{2}\boldsymbol{s} : \boldsymbol{s}$ or the norm $\|\boldsymbol{s}\| := \boldsymbol{s} : \boldsymbol{s}$ of the deviatoric stress tensor $\boldsymbol{s}$.

The discontinuity angle $\theta^{\rm cr}$ is given from Eq. (4.2) as

$$\sin^2\theta^{\rm cr} = -\frac{s_2}{s_1 - s_2}, \qquad \cos^2\theta^{\rm cr} = \frac{s_1}{s_1 - s_2} \tag{4.19}$$

for the in-plane principal values s_i ($i = 1, 2$) of the deviatoric stress tensor $\boldsymbol{s}$.

4.5.1. Plane stress

In the case of plane stress ($\sigma_3 = 0$), it follows that

$$\sin^2\theta^{\rm cr} = \frac{\sigma_1 - 2\sigma_2}{3(\sigma_1 - \sigma_2)}, \qquad \cos^2\theta^{\rm cr} = \frac{2\sigma_1 - \sigma_2}{3(\sigma_1 - \sigma_2)} \tag{4.20}$$

if the conditions $\sigma_1 \ge \frac{1}{2}\sigma_2$ and $\sigma_1 \ge 2\sigma_2$ are satisfied. The resulting discontinuity angles $\theta^{\rm cr}$ for different stress ratios σ_1/σ_2 are summarized in Table 1 and depicted in Fig. 10.

With the discontinuity angle (4.20), the corresponding normal and tangential tractions (t_n, t_m) are evaluated as

$$t_n = \sigma_{nn} = \frac{2}{3}(\sigma_1 + \sigma_2), \qquad t_m^2 = \sigma_{nm}^2 = -s_1 s_2 \tag{4.21}$$

so that

$$J_2 = \frac{1}{3}\big(\sigma_1^2 + \sigma_2^2 - \sigma_1\sigma_2\big) = \frac{1}{4}t_n^2 + t_m^2 \tag{4.22}$$

Substitution of the result (4.22) into Eq. (4.18) yields

$$f(\boldsymbol{t}, q) = \sqrt{3\Big(\frac{1}{4}t_n^2 + t_m^2\Big)} - q \le 0 \tag{4.23}$$

The above traction-based failure criterion can also be derived from the definition (4.7). For the equi-biaxial tension/compression stress state, i.e., $\sigma_2 = -\sigma_1$ and $t_n = 0$, the expected mode II failure criterion is recovered.

Remark 4.4. For the cases $\sigma_1 \le \frac{1}{2}\sigma_2$ or $\sigma_1 \le 2\sigma_2$, the discontinuity angles $\theta^{\rm cr}$ in Eq. (B.1) apply. Accordingly, the modified stress- and traction-based failure criteria are given from Eqs. (B.2) and (B.3), respectively, i.e.,

$$\hat{F}(\boldsymbol{\sigma}, q) = \begin{cases} \dfrac{\sqrt{3}}{2}\sigma_1 - q & 0 < \sigma_2 < \sigma_1 < 2\sigma_2 \\ -\dfrac{\sqrt{3}}{2}\sigma_2 - q & 2\sigma_1 < \sigma_2 < \sigma_1 < 0 \end{cases} \tag{4.24a}$$

$$f(\boldsymbol{t}, q) = \frac{\sqrt{3}}{2}\big|t_n\big| - q \le 0 \tag{4.24b}$$

The above modified failure criteria are also illustrated in Fig. 10.

4.5.2. Plane strain

In the case of plane strain, the extra condition (4.4) requires that

$$\hat{\Lambda}_3 = 0 \qquad \Longrightarrow \qquad s_3 = 0, \qquad \sigma_3 = \frac{1}{2}(\sigma_1 + \sigma_2) \tag{4.25}$$

That is, $\eta_1 = 1/2$ and $\eta_2 = 0$ in the out-of-plane principal stress (4.4).

Upon the above stress state, it follows that $s_1 = -s_2$ such that Eq. (4.19) gives

$$\sin^2\theta^{\rm cr} = -\frac{s_2}{s_1 - s_2} = \frac{1}{2} \qquad \Longrightarrow \qquad \theta^{\rm cr} = 45^\circ \tag{4.26}$$

Table 1
Discontinuity angles θ^{cr} for the von Mises criterion in the condition of plane stress.

	Stress ratio σ_1/σ_2							
	−1: −2	−1: −5	0: −1	1: −5	1: −1	1: 0	1: 0.25	1: 0.5
θ^{cr}	90.00°	60.00°	54.74°	51.42°	45.00°	35.26°	28.12°	0.00°

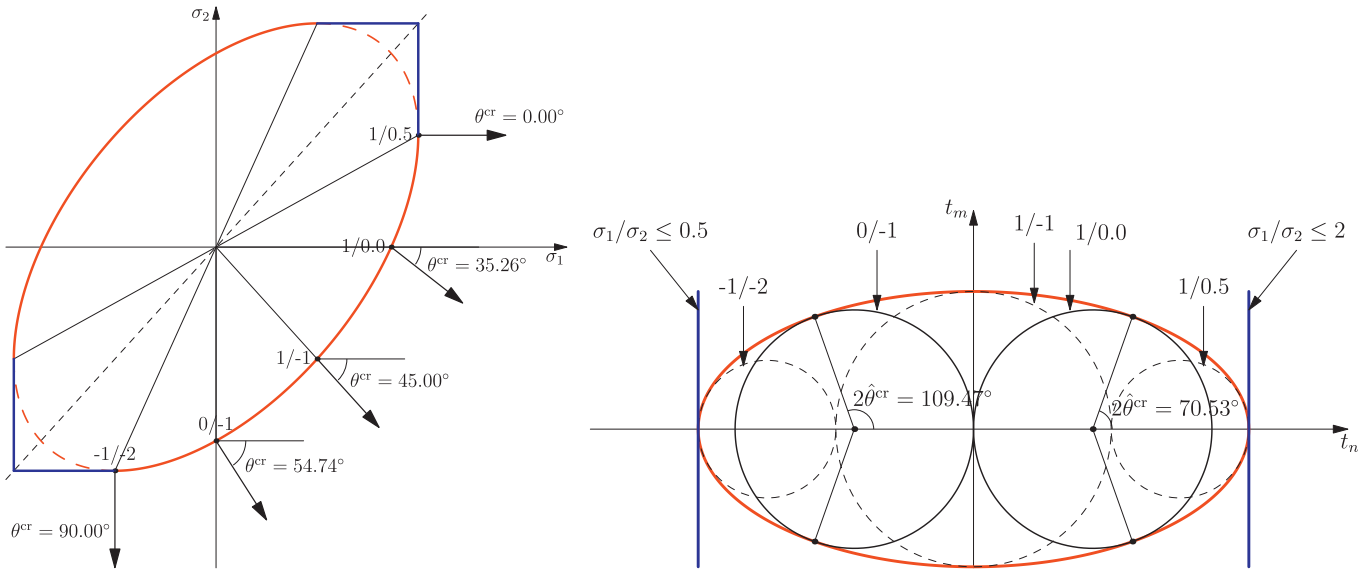

(a) Principal stress space (b) Traction space

Fig. 10. Discontinuity angles of the von Mises criterion in the condition of plane stress.

As can be seen, in the condition of plane strain the discontinuity angle is fixed as $\theta^{cr} = 45°$ independently of the stress ratio σ_1/σ_2. This result, different from that given from the discontinuous bifurcation analysis (Runesson et al., 1991), was recently confirmed by the numerical simulations (Cervera et al., 2012).

For the discontinuity angle (4.26), the traction-based failure function (4.7) is expressed as

$$f(\boldsymbol{t}, q) = \sqrt{3}\,\left|t_m\right| - q \le 0 \tag{4.27}$$

As expected, for the von Mises criterion in the plane strain condition a pure mode II discontinuity forms upon strain localization, whatever the stress state is.

Remark 4.5. In the case of plane strain, with the elastic out-of-plane stress (4.3) the initial elastic limit surface $\hat{F}(\boldsymbol{\sigma}, q^0) = 0$ is expressed as

$$\sqrt{\left(1 - \nu_0 + \nu_0^2\right)\left(\sigma_1^2 + \sigma_2^2\right) - \left(1 + 2\nu_0 - 2\nu_0^2\right)\sigma_1\sigma_2} = q^0 \tag{4.28}$$

Contrariwise, with the out-of-plane stress (4.25) upon plane strain localization, the failure criterion $\hat{F}(\boldsymbol{\sigma}, q) \le 0$ becomes two parallel straight lines, i.e.,

$$\hat{F}(\boldsymbol{\sigma}, q) = \frac{\sqrt{3}}{2}\,\left|\sigma_1 - \sigma_2\right| - q \le 0 \tag{4.29}$$

As depicted in Fig. 11, only for the particular case $\nu_0 = 0.5$ or $\sigma_2 = -\sigma_1$, can strain localization occur at the onset of strain softening. For all other cases, the elastic limit surface (4.28) will be reached first and strain softening occurs accompanied with (continuous) inelastic deformations. Only when sufficient re-orientation of the principal strain directions is completed and the plane strain localization condition (4.25) is fulfilled, strain localization sets in motion and a strong (regularized) discontinuity forms.

4.6. Example: Drucker–Prager criterion

Finally, let us consider the Drucker–Prager criterion expressed as

$$\hat{F}(\boldsymbol{\sigma}, q) = \frac{1}{1+\alpha}\left(\alpha I_1 + \sqrt{3J_2}\right) - q \le 0 \tag{4.30}$$

where the parameter $\alpha = (\rho - 1)/(\rho + 1) \in [0, 1)$ is related to the ratio $\rho := f_c/f_t \ge 1$ between the uniaxial compressive strength f_c and the tensile one f_t.

The discontinuity angle θ^{cr} is computed from Eq. (4.2) as

$$\sin^2\theta^{cr} = -\frac{\sqrt{2/3}\,\alpha\left\|\boldsymbol{s}\right\| + s_2}{s_1 - s_2}, \qquad \cos^2\theta^{cr} = \frac{\sqrt{2/3}\,\alpha\left\|\boldsymbol{s}\right\| + s_1}{s_1 - s_2} \tag{4.31}$$

where s_1 and s_2 denote the in-plane principal values of the deviatoric stress tensor $\boldsymbol{s}$.

Remark 4.6. For an activated discontinuity, it follows from the fact $\hat{F}(\boldsymbol{\sigma}, q) = 0$ that

$$\sqrt{\frac{2}{3}}\,\left\|\boldsymbol{s}\right\| = \frac{2}{3}\left[\left(1+\alpha\right)q - \alpha I_1\right] \ge 0 \tag{4.32}$$

This relation is useful for later derivation of the traction-based failure criterion $f(\boldsymbol{t}, q) \le 0$.

Table 2
Discontinuity angles θ^{cr} for the Drucker–Prager criterion in the condition of plane stress.

f_c/f_t	Stress ratio σ_1/σ_2									
	−1: −1.24	−1: −2	−1: −5	0: −1	1: −5	1: −1	1: −0.5	1: −0.25	1: −0.15	1: 0	1 : 0.19
2.00	90.00°	51.65°	44.74°	41.81°	39.52°	33.68°	29.90°	26.30°	24.15°	19.47°	0.00°
3.00	43.48°	40.55°	37.35°	35.26°	33.32°	27.37°	22.82°	17.90°	14.51°	0.00°	0.00°
4.00	–	33.66°	32.69°	31.09°	29.33°	23.07°	17.62°	10.53°	0.00°	0.00°	0.00°

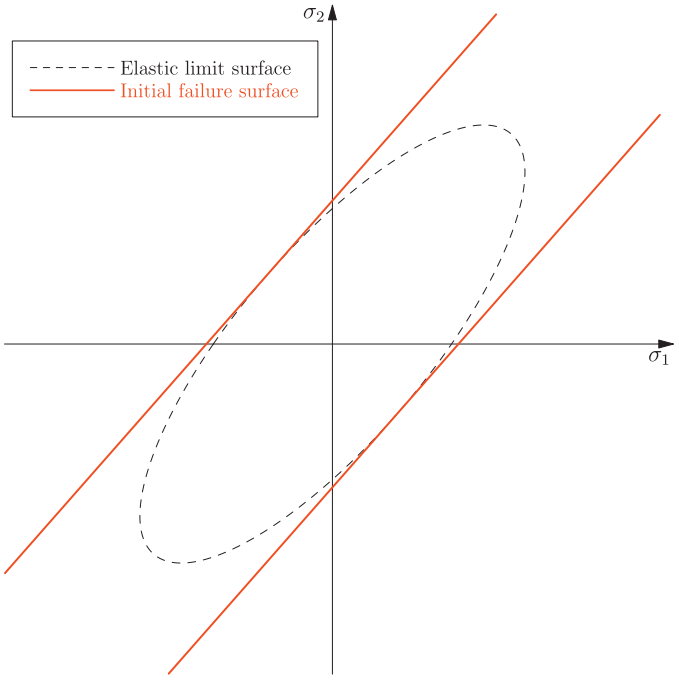

Fig. 11. Elastic limit surface and initial failure surface of the von Mises criterion in the condition of plane strain.

4.6.1. Plane stress

In the case of plane stress ($\sigma_3 = 0$), the results (4.31) become

$$\sin^2\theta^{cr} = -\frac{(2\sigma_2-\sigma_1)+2\alpha\sqrt{\sigma_1^2+\sigma_2^2-\sigma_1\sigma_2}}{3(\sigma_1-\sigma_2)} \tag{4.33a}$$

$$\cos^2\theta^{cr} = \frac{(2\sigma_1-\sigma_2)+2\alpha\sqrt{\sigma_1^2+\sigma_2^2-\sigma_1\sigma_2}}{3(\sigma_1-\sigma_2)} \tag{4.33b}$$

if the conditions $\sigma_1 \geq \tilde{\alpha}_1\sigma_2$ and $\sigma_1 \geq \sigma_2/\tilde{\alpha}_2$ are satisfied, with the parameters $\tilde{\alpha}_1$ and $\tilde{\alpha}_2$ expressed as $\tilde{\alpha}_{1,2} := \frac{1}{2}[1 \pm \alpha\sqrt{3/(1-\alpha^2)}]$. Similarly, the exceptional cases are obtained from the arguments in Appendix B.

The above discontinuity angle θ^{cr} is summarized in Table 2 for different values of the stress ratio σ_1/σ_2 and model parameter α.

With the discontinuity angle (4.33), the traction-based failure criterion can be determined as (see Appendix C for the derivation)

$$t_m^2 - \frac{4\alpha^2-1}{4(1-\alpha^2)}t_n^2 + \frac{\alpha}{1-\alpha}qt_n - \frac{1+\alpha}{3(1-\alpha)}q^2 \leq 0 \tag{4.34}$$

As depicted in Fig. 12, the following three cases can be identified for the stress-based failure criterion (4.30) and its projected traction-based counterpart (4.34) regarding the model parameter $\alpha \in [0, 1)$ (or, equivalently, $\rho \geq 1$):

- $0 \leq \alpha < 1/2$ or $1 \leq \rho < 3$: The stress-based failure criterion (4.30) is an ellipse on the $\sigma_1 - \sigma_2$ plane and the traction-based counterpart (4.34) also defines an ellipse on the $t_n - t_m$ plane

$$t_m^2 + \frac{1-4\alpha^2}{4(1-\alpha^2)}\left[t_n + \frac{2\alpha(1+\alpha)}{1-4\alpha^2}q\right]^2 - \frac{(1+\alpha)^2}{3(1-4\alpha^2)}q^2 \leq 0 \tag{4.35}$$

  The classical von Mises criterion belongs to this type (i.e., $\alpha = 0$).
- $\alpha = 1/2$ or $\rho = 3$: The stress-based failure criterion (4.30) defines a parabola on the $\sigma_1 - \sigma_2$ plane, while the traction-based counterpart (4.34) becomes

$$t_m^2 + qt_n - q^2 \leq 0 \tag{4.36}$$

  which is a parabola on the $t_n - t_m$ plane.
- $1/2 < \alpha < 1$ or $\rho > 3$: The stress-based failure criterion (4.30) defines a hyperbola on the $\sigma_1 - \sigma_2$ plane. Similarly, the traction-based counterpart (4.34) is a hyperbola on the $t_n - t_m$ plane, with the left branch of interest given by

$$\tan\varphi \cdot t_n + \sqrt{t_m^2 + \omega^2 q^2} - c \leq 0 \tag{4.37}$$

  where the parameters $\tan\varphi$, ω and c are expressed as

$$\tan\varphi = \sqrt{\frac{4\alpha^2-1}{4(1-\alpha^2)}}, \qquad \omega = \frac{1+\alpha}{\sqrt{3(4\alpha^2-1)}},$$
$$c = \frac{\alpha(1+\alpha)}{\sqrt{(4\alpha^2-1)(1-\alpha^2)}}q \tag{4.38}$$

  This hyperbolic failure criterion asymptotically approaching to a Mohr–Coulomb one has been widely adopted in the modeling of mixed-mode failure in quasi-brittle solids (Carol et al., 1997; Most and Bucher, 2007).

Remark 4.7. For the parameter $\alpha \in [1/2, 1)$, the Drucker–Prager failure criterion (4.30) defines an open surface in the principle $\sigma_1 - \sigma_2$ space. Accordingly, there exists a limit value for the discontinuity angle θ^{cr}. For the parabolic failure criterion (i.e., $\alpha = 1/2$), it follows that

$$\lim_{\sigma_2\to\sigma_1<0}\sin^2\theta^{cr} = \lim_{\sigma_2\to\sigma_1<0} -\frac{(2\sigma_2-\sigma_1)+\sqrt{\sigma_1^2+\sigma_2^2-\sigma_1\sigma_2}}{3(\sigma_1-\sigma_2)} = \frac{1}{2} \tag{4.39}$$

Namely, the limit discontinuity angle is $\lim_{\sigma_2\to\sigma_1<0}\theta^{cr} = 45^\circ$. For the hyperbolic one with $\alpha \in (1/2, 1)$, the admissible stress ratio σ_1/σ_2 in the compression-compression quadrant (i.e., $\sigma_1 < 0$ and $\sigma_2 < 0$) is constrained by the parameter α, and so is the discontinuity angle θ^{cr}, i.e.,

$$\sin\theta^{cr} \leq \sqrt{\frac{(1+2\alpha^2)\sigma_1/\sigma_2 - 2(1-\alpha^2)}{3(\sigma_1/\sigma_2-1)}} \quad \text{with}$$
$$\frac{\sigma_1}{\sigma_2} \leq \frac{1+2\alpha^2-\sqrt{3(4\alpha^2-1)}}{2(1-\alpha^2)} \tag{4.40}$$

For instance, it follows that $0^\circ \leq \theta^{cr} \leq 33.74^\circ$ for the parameter $\rho = 4.0$ (or, equivalently, $\alpha = 0.6$).

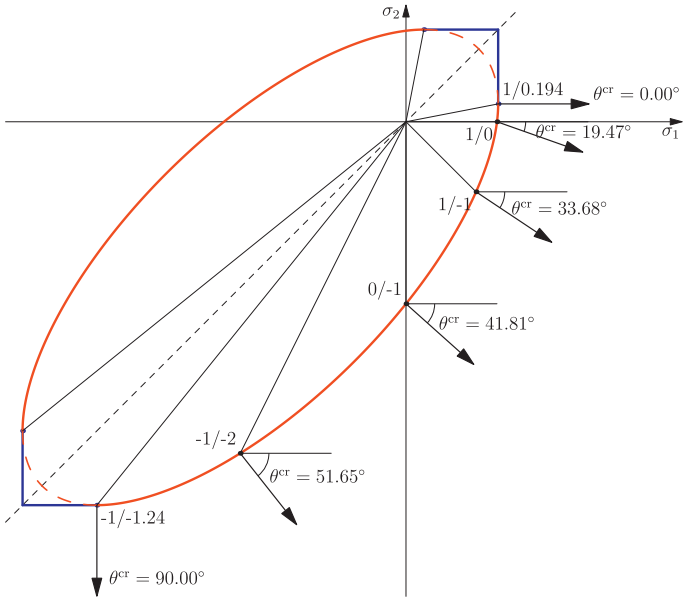

(a) Elliptic type ($\rho = 2.0$)

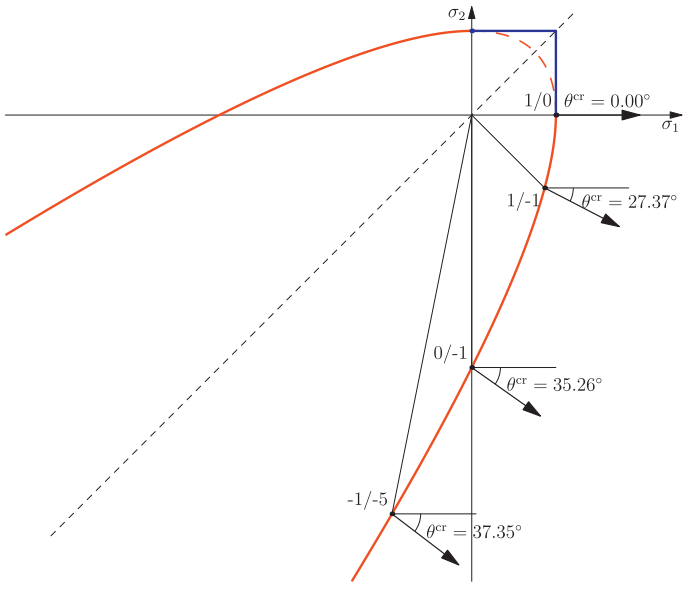

(b) Parabolic type ($\rho = 3.0$)

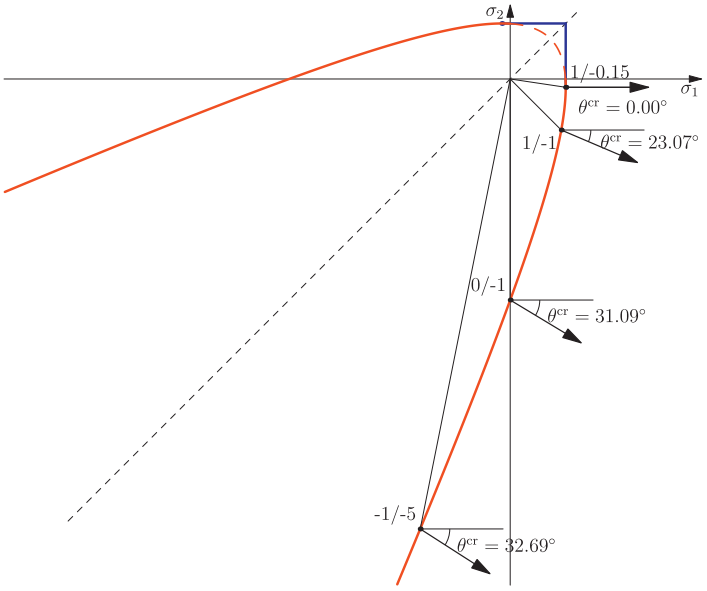

(c) Hyperbolic type ($\rho = 4.0$)

Fig. 12. The Drucker–Prager criteria of different types in the condition of plane stress.

4.6.2. Plane strain

In the case of plane strain, the extra condition (4.4) gives the following out-of-plane stress $\sigma_3 \neq 0$, i.e.,

$$\alpha + \sqrt{\frac{3}{2}}\frac{1}{\|\boldsymbol{s}\|}s_3 = 0 \quad \Longrightarrow \quad \sigma_3 = \frac{2\alpha^2+1}{2\left(1-\alpha^2\right)}\left(\sigma_1+\sigma_2\right) - \frac{\alpha}{1-\alpha}q \tag{4.41}$$

As the trace $\mathrm{tr}\boldsymbol{s}$ vanishes, it follows that

$$s_1 + s_2 = -s_3 = \sqrt{\frac{2}{3}}\,\alpha\,\|\boldsymbol{s}\| \geq 0 \quad \text{or} \quad s_1^2 + \frac{6-4\alpha^2}{3-4\alpha^2}\,s_1 s_2 + s_2^2 = 0 \tag{4.42}$$

Accordingly, the discontinuity angle (4.33) is determined from

$$\sin^2\theta^{cr} = -\frac{s_1+2s_2}{s_1-s_2} = -\frac{\alpha_s+2}{\alpha_s-1},$$
$$\cos^2\theta^{cr} = \frac{2s_1+s_2}{s_1-s_2} = \frac{2\alpha_s+1}{\alpha_s-1} \tag{4.43}$$

for the ratio $\alpha_s := s_1/s_2$ given from the relation (4.42)

$$\alpha_s := \frac{s_1}{s_2} = \frac{2\alpha^2-3-2\alpha\sqrt{3\left(1-\alpha^2\right)}}{3-4\alpha^2} \in \left[-2,-1\right] \tag{4.44}$$

The above result holds if the following condition

$$2s_1+s_2 \geq 0, \quad s_1+2s_2 \leq 0 \quad \Longleftrightarrow \quad 0 \leq \alpha \leq \frac{1}{2} \tag{4.45}$$

Table 3
Discontinuity angles θ^{cr} for the Drucker–Prager criterion in the condition of plane strain.

Strength ratio f_c/f_t	1.0	1.50	2.00	2.50	3.00
Discontinuity angle θ^{cr}	45.00°	34.65°	26.12°	17.38°	0.00°

is satisfied. Compared to the result (4.33) for the case of plane stress, the discontinuity angle θ^{cr} determined from Eqs. (4.43) and (4.44) depends only on the model parameter $\alpha \in [0, 1/2]$; see Table 3. Note that the result for the von Mises criterion is recovered for the parameter $\alpha = 0$.

Again, the above analytical results, different from those obtained from the discontinuous bifurcation analysis (Runesson et al., 1991), were numerically confirmed by Cervera et al. (2015).

With the discontinuity angle (4.43), the traction-based failure criterion (4.7) can be derived as (see Appendix C)

$$t_m^2 - \frac{3\alpha^2}{1-4\alpha^2}\left(t_n - \frac{1+\alpha}{3}q\right)^2 \le 0 \tag{4.46}$$

with the left branch of interest expressed as

$$t_n \cdot \tan\varphi + |t_m| - c \le 0 \tag{4.47}$$

where the friction angle φ and the cohesion c are given by

$$\tan\varphi = \alpha\sqrt{\frac{3}{1-4\alpha^2}}, \qquad c = \frac{1+\alpha}{\sqrt{3\left(1-4\alpha^2\right)}}q \tag{4.48a}$$

or, equivalently,

$$\alpha = \frac{\tan\varphi}{\sqrt{3+4\tan^2\varphi}}, \qquad \left(1+\alpha\right)q = \frac{3c}{\sqrt{3+4\tan^2\varphi}} \tag{4.48b}$$

That is, in the case of plane strain, the material characterized by the Drucker–Prager model localizes into a Mohr–Coulomb discontinuity. The above relations (4.48) are exactly the matching conditions under which the Drucker–Prager and Mohr–Coulomb models give identical limit load for *perfectly-plastic* materials in the case of plane strain. Furthermore, upon satisfaction of these plane strain matching conditions, both models produce identical energy dissipation (Chen, 1994).

Remark 4.8. In the case of plane strain, on the one hand, calling for the out-of-plane stress (4.3) the elastic limit surface $\hat{F}(\boldsymbol{\sigma}, q^0) = 0$ of the Drucker–Prager criterion (4.30) is given by

$$\frac{1}{1+\alpha}\Big[\alpha\left(1+\nu_0\right)\left(\sigma_1+\sigma_2\right) + \sqrt{\left(1-\nu_0+\nu_0^2\right)\left(\sigma_1^2+\sigma_2^2\right) - \left(1+2\nu_0-2\nu_0^2\right)\sigma_1\sigma_2}\Big] = q^0 \tag{4.49}$$

The above elastic limit surface can be either an ellipse for $\alpha < (1/2-\nu_0)/(1+\nu_0)$, a parabola for $\alpha = (1/2-\nu_0)/(1+\nu_0)$, or a hyperbola for $\alpha > (1/2-\nu_0)/(1+\nu_0)$ on the $\sigma_1-\sigma_2$ plane, respectively. On the other hand, for the plane strain localization condition (4.41), the Drucker–Prager criterion (4.30) becomes

$$\left|\sigma_1-\sigma_2\right| = \sqrt{\frac{3}{1-\alpha^2}}\left[\frac{2}{3}\left(1+\alpha\right)q - \alpha\left(\sigma_1+\sigma_2\right)\right] \ge 0 \tag{4.50}$$

It follows from Eqs. (4.3) and (4.44) that only for the particular stress state

$$\frac{\sigma_1}{\sigma_2} = \frac{2-\nu_0+\alpha_s\left(1+\nu_0\right)}{1+\nu_0+\alpha_s\left(2-\nu_0\right)} \tag{4.51}$$

can strain localization occur at the onset of softening; see Fig. 13. For all other cases, continuous inelastic deformations and reorientation of the principal strain directions have to take place until the condition (4.41) or (4.44) is reached, after which strain localization occurs with a strong discontinuity.

5. Conclusions

Aiming for the modeling of localized failure in quasi-brittle solids, this paper presents a unified elastoplastic-damage framework based on the framework of irreversible thermodynamics. Both concepts of degradation strain rate and damage strain are incorporated to develop an elastoplastic damage model, with evolution laws for the involved internal variables characterized by a dissipative flow tensor. To explore its use in the modeling of strong or regularized discontinuities, a novel strain localization analysis is proposed to prognosticate their occurrence based on continuity of tractions on and across the discontinuity (band). The resulting kinematic localization condition is in general more demanding than the classical discontinuous bifurcation one. The kinematic constraint, on the one hand, is sufficient to guarantee the traction continuity and stress boundedness; on the other hand, it is necessary to reproduce the consistent loading/unloading deformation states upon strain localization in quasi-brittle solids and to guarantee formation of a fully softened discontinuity.

For such strain localization to occur with a strong (or regularized) discontinuity, it is necessary that Maxwell's kinematics of the discontinuity (band) be reproduced in an appropriate manner. Regarding the elastoplastic damage model considered in this work, the components of the dissipative flow tensor in the directions orthogonal to the discontinuity orientation have to vanish upon strain localization. Satisfaction of this kinematic constraint allows developing a localized plastic-damage model for the inelastic discontinuity (band), with both its orientation and the corresponding traction-based failure criterion determined consistently from the given stress-based counterpart. The projected discontinuity approach so derived avoids introducing the cohesive zone model in an *ad hoc* manner. In particular, the involved model parameters can be calibrated from available macroscopic material test data as demonstrated in our previous work (Cervera and Wu, 2015; Wu and Cervera, 2015). Furthermore, the right instant for the occurrence of strong (or regularized) discontinuities and the introduction of localized models can also be identified.

The aforementioned general results are particularized to 2D conditions of plane stress and plane strain. The discontinuity orientation and the corresponding traction-based failure criterion are obtained in closed-form for a given stress-based counterpart. Finally, the Rankine, Mohr–Coulomb, von Mises (J_2) and Drucker–Prager criteria are analyzed as illustrative examples, with the analytical discontinuity angles coincident with those obtained from numerical simulations. It is found that in the case of plane stress, strain localization with a strong (regularized) discontinuity can occur at the onset of strain softening. Contrariwise, owing to the extra out-of-plane kinematic constraint, in the condition of plane strain some continuous inelastic deformations and substantial reorientation of principal strain directions have to take place prior to strain localization.

So far only homogeneous materials with a single discontinuity have been considered. In heterogeneous materials like reinforced concrete or other composites, multiple discontinuities may be initiated, possibly with branching. In such complex situations, orientation and spacing of the discontinuities are affected strongly by the reinforcing phases. It would be instructive to investigate the application and extension of the current method to more challenging issues.

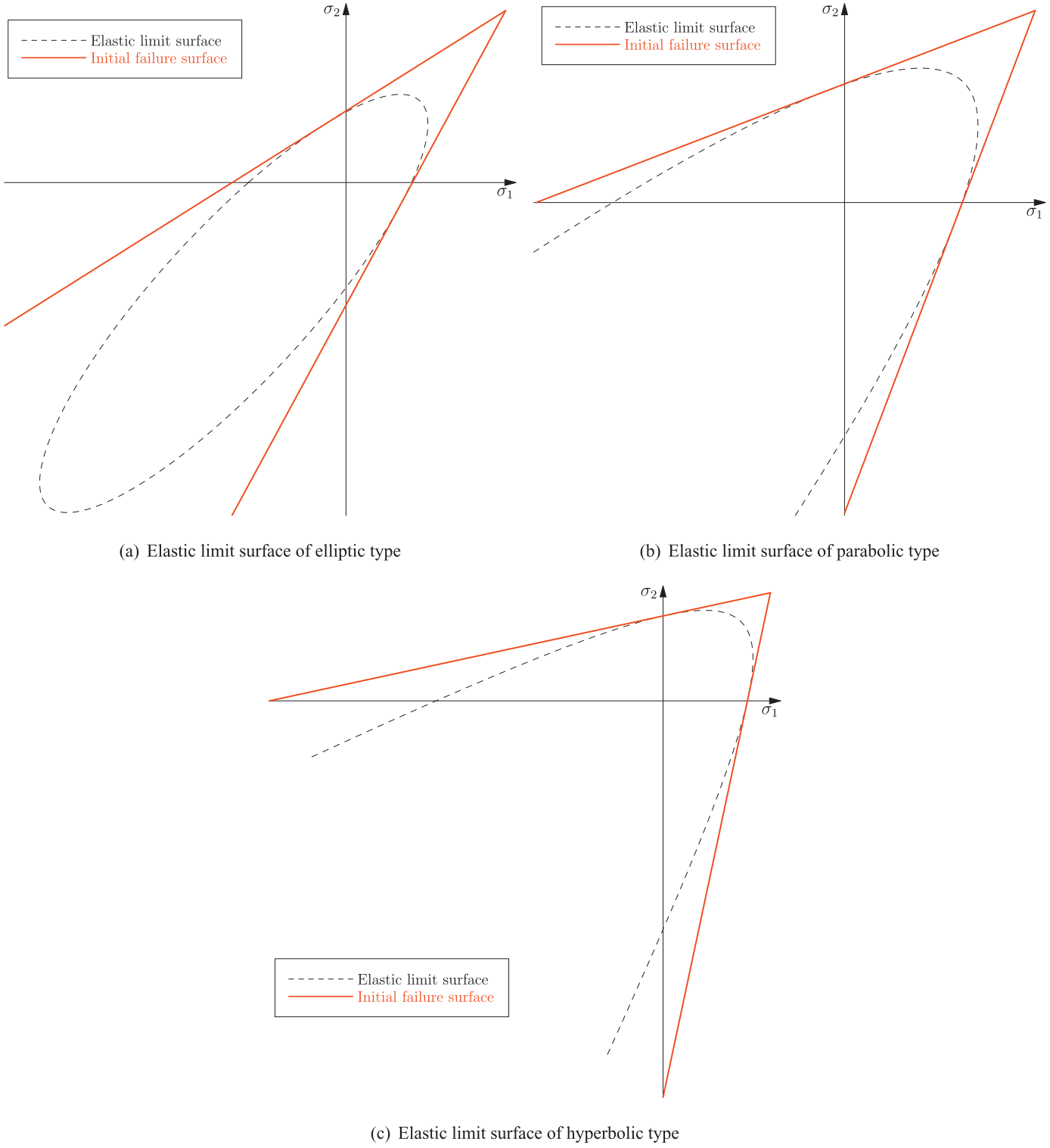

(a) Elastic limit surface of elliptic type

(b) Elastic limit surface of parabolic type

(c) Elastic limit surface of hyperbolic type

Fig. 13. Elastic limit surface and initial failure surface of the Drucker–Prager criterion in the condition of plane strain.

Acknowledgments

Support from the National Natural Science Foundation of China (51222811), the State Key Laboratory of Subtropical Building Science (2015ZB24, 2016KB12) and the Fundamental Research Funds for the Central University (2015ZZ078) to the first author (J.Y. Wu) is acknowledged. Support from the Spanish Ministry of Economy and Competitivity under the project Enhanced Accuracy Computational Framework for Strain Localization and Failure Mechanisms (EACY) – is acknowledged by the second author (M. Cervera).

Appendix A. Mohr's maximization postulate

Mohr's maximization postulate (Mohr, 1900) assumes that a discontinuity (band) is initiated on the orientation $\boldsymbol{n}(\hat{\boldsymbol{\theta}}^{\mathrm{cr}})$ upon which the tractions maximize the failure function $\hat{f}\big[\boldsymbol{t}(\boldsymbol{\theta}), q\big]$, i.e.,

$$\hat{\boldsymbol{\theta}}^{\mathrm{cr}} = \arg\max \hat{f}\big[\boldsymbol{t}(\boldsymbol{\theta}), q\big] = \arg\max \hat{f}\big[\boldsymbol{\sigma}\cdot\boldsymbol{n}(\boldsymbol{\theta}), q\big] \tag{A.1}$$

for the characteristic angles $\hat{\boldsymbol{\theta}}^{\mathrm{cr}}$. Mathematically, the following stationarity condition holds

$$\frac{\partial \hat{f}}{\partial \boldsymbol{\theta}}\Big|_{\hat{\boldsymbol{\theta}}^{\mathrm{cr}}} = \left(\hat{\boldsymbol{\gamma}}\cdot\frac{\partial \boldsymbol{t}}{\partial \boldsymbol{\theta}}\right)_{\hat{\boldsymbol{\theta}}^{\mathrm{cr}}} = \left(\hat{\gamma}_n\frac{\partial t_n}{\partial \boldsymbol{\theta}} + \hat{\gamma}_m\frac{\partial t_m}{\partial \boldsymbol{\theta}} + \hat{\gamma}_p\frac{\partial t_p}{\partial \boldsymbol{\theta}}\right)_{\hat{\boldsymbol{\theta}}^{\mathrm{cr}}} = \boldsymbol{0} \tag{A.2}$$

together with a negative-definite Hessian matrix $\partial^2\hat{f}/\partial\boldsymbol{\theta}^2$ at the discontinuity angles $\hat{\boldsymbol{\theta}}^{\mathrm{cr}}$.

As the dissipative flow tensor $\boldsymbol{\Lambda} := \partial\hat{f}/\partial\boldsymbol{\sigma}$ is co-axial to the stress $\boldsymbol{\sigma}$ (Itskov, 2007), it follows that

$$\boldsymbol{\Lambda} : \frac{\partial \boldsymbol{\sigma}}{\partial \boldsymbol{\theta}} = 2\sum_{i=1}^{3}\Lambda_i\sigma_i\left(\boldsymbol{v}_i\cdot\frac{\partial \boldsymbol{v}_i}{\partial \boldsymbol{\theta}}\right) = 0 \tag{A.3}$$

where the identity $\boldsymbol{v}_i\cdot\left(\partial\boldsymbol{v}_i/\partial\boldsymbol{\theta}\right) = 0$, resulting from the relation $\boldsymbol{v}_i\cdot\boldsymbol{v}_i = 1$, has been considered. Recalling the relations (3.18), the stationarity condition (A.2) becomes (Wu and Cervera, 2015)

$$\frac{\partial \hat{f}}{\partial \boldsymbol{\theta}}\Big|_{\hat{\boldsymbol{\theta}}^{\mathrm{cr}}} = -\left(\Lambda_{mm}\frac{\partial \sigma_{mm}}{\partial \boldsymbol{\theta}} + 2\Lambda_{mp}\frac{\partial \sigma_{mp}}{\partial \boldsymbol{\theta}} + \Lambda_{pp}\frac{\partial \sigma_{pp}}{\partial \boldsymbol{\theta}}\right)_{\hat{\boldsymbol{\theta}}^{\mathrm{cr}}} = \boldsymbol{0} \tag{A.4}$$

As the failure function $\hat{f}(\boldsymbol{t}, q) \le 0$ depends only on the tractions $\boldsymbol{t} := \{\sigma_{nn}, \sigma_{nm}, \sigma_{np}\}^{\mathrm{T}}$, the condition (A.4) is fulfilled for arbitrary values of the remaining stress components (σ_{mm}, σ_{mp}, σ_{pp}), i.e.,

$$\Lambda_{mm}(\hat{\boldsymbol{\theta}}^{\mathrm{cr}}) = 0, \qquad \Lambda_{pp}(\hat{\boldsymbol{\theta}}^{\mathrm{cr}}) = 0, \qquad \Lambda_{mp}(\hat{\boldsymbol{\theta}}^{\mathrm{cr}}) = 0 \tag{A.5}$$

The above relations correspond exactly to the kinematic constraints (3.19).

If the solution to Eq. (A.5) does not exist, the discontinuity angles $\hat{\boldsymbol{\theta}}^{\mathrm{cr}}$ should be determined from another set of solution to Eq. (A.4)

$$\frac{\partial \sigma_{mm}}{\partial \boldsymbol{\theta}}\Big|_{\hat{\boldsymbol{\theta}}^{\mathrm{cr}}} = 0, \qquad \frac{\partial \sigma_{mp}}{\partial \boldsymbol{\theta}}\Big|_{\hat{\boldsymbol{\theta}}^{\mathrm{cr}}} = 0, \qquad \frac{\partial \sigma_{pp}}{\partial \boldsymbol{\theta}}\Big|_{\hat{\boldsymbol{\theta}}^{\mathrm{cr}}} = 0 \tag{A.6}$$

Contrariwise, if the solution to the kinematic constraints (3.19) does not exist for the stress-based material model, strain localization into a strong (regularized) discontinuity cannot occur. In this exceptional situation, the given stress-based failure criterion can be modified based on the solution to Eq. (A.6) so that both families of approaches are completely equivalent as shown in Wu and Cervera (2014b; 2015); see Appendix B for the 2D cases.

Appendix B. Exceptional 2D cases

For 2D cases in which $\hat{\Lambda}_2 > 0$ or $\hat{\Lambda}_1 < 0$, the discontinuity angle θ^{cr} cannot be determined from Eq. (4.2). It implies that strain localization into a strong (regularized) discontinuity cannot occur for the given stress-based failure criterion $\hat{F}(\boldsymbol{\sigma}, q) \le 0$.

In this exceptional situation, some necessary modifications should be made in such a way that strain localization into a strong (regularized) discontinuity may still occur in the stress-based inelastic solid and the resulting projected discontinuity approach is completely equivalent to a traction-based strong/regularized one. That is, the discontinuity angle is given from the solution to Eq. (A.6), i.e.,

$$\sin(2\theta^{\mathrm{cr}}) = 0 \qquad \theta^{\mathrm{cr}} = \begin{cases} 0 & \widehat{\Lambda}_1 > \widehat{\Lambda}_2 > 0 \\ \pi/2 & \widehat{\Lambda}_2 < \widehat{\Lambda}_1 < 0 \end{cases} \tag{B.1}$$

which corresponds to the limit values $\hat{\Lambda}_2 = 0$ and $\hat{\Lambda}_1 = 0$ in Eq. (4.2), respectively.

Accordingly, the given stress-based failure function $\hat{F}(\boldsymbol{\sigma}, q)$ is modified as

$$\hat{F}(\boldsymbol{\sigma}, q) = \begin{cases} \dfrac{1}{M}\left[\left(\hat{\Lambda}_1\Big|_{\hat{\Lambda}_2=0}\right)\sigma_1 - \hat{h}\cdot q\right] & \hat{\Lambda}_1 > \hat{\Lambda}_2 > 0 \\ \dfrac{1}{M}\left[\left(\hat{\Lambda}_2\Big|_{\hat{\Lambda}_1=0}\right)\sigma_2 - \hat{h}\cdot q\right] & \hat{\Lambda}_2 < \hat{\Lambda}_1 < 0 \end{cases} \tag{B.2}$$

As depicted in Figs. 10(a) and 12, this strategy introduces tension- and compression-extensions into the original stress-based failure criterion $\hat{F}(\boldsymbol{\sigma}, q) \le 0$. Similarly, the projected traction-based failure function $f(\boldsymbol{t}, q)$ is given by

$$f(\boldsymbol{t}, q) = \begin{cases} \dfrac{1}{M}\left[\left(\hat{\Lambda}_1\Big|_{\hat{\Lambda}_2=0}\right)t_n - \hat{h}\cdot q\right] & \hat{\Lambda}_1 > \hat{\Lambda}_2 > 0 \\ \dfrac{1}{M}\left[\left(\hat{\Lambda}_2\Big|_{\hat{\Lambda}_1=0}\right)t_n - \hat{h}\cdot q\right] & \hat{\Lambda}_2 < \hat{\Lambda}_2 < 0 \end{cases} \tag{B.3}$$

where the tangential traction is removed from the failure criterion (4.7). With the above modifications, the stress- and traction-based models are completely equivalent to each other as shown in Wu and Cervera (2014b; 2015).

Appendix C. Traction-based failure criteria for the Drucker–Prager model

In the case of plane stress, for the discontinuity angle (4.33) it follows that

$$t_n = \frac{2}{3}\Big[\alpha\big(1+\alpha\big)q + \big(1-\alpha^2\big)\big(\sigma_1+\sigma_2\big)\Big] \tag{C.1a}$$

$$t_m^2 = -\Big(\sqrt{2/3}\,\alpha\,\|\boldsymbol{s}\| + s_1\Big)\Big(\sqrt{2/3}\,\alpha\,\|\boldsymbol{s}\| + s_2\Big) \tag{C.1b}$$

Accordingly, the normal and tangential components (γ_n, γ_m) in Eq. (4.6) become

$$\gamma_n = \frac{1}{\big(1+\alpha\big)\sqrt{2/3}\,\|\boldsymbol{s}\|}\,\frac{\big(1-4\alpha^2\big)t_n + 2\alpha\big(1+\alpha\big)q}{2\big(1-\alpha^2\big)} \tag{C.2a}$$

$$\gamma_m = \frac{1}{\big(1+\alpha\big)\sqrt{2/3}\,\|\boldsymbol{s}\|}\,2t_m \tag{C.2b}$$

where the norm $\|\boldsymbol{s}\|$ is evaluated from Eq. (4.32) as

$$\sqrt{\frac{2}{3}}\,\|\boldsymbol{s}\| = \frac{1}{1-\alpha^2}\Big[\frac{2}{3}\big(1+\alpha\big)q - \alpha t_n\Big] \ge 0 \tag{C.3}$$

Therefore, the definition (4.7) gives the following traction-based failure function

$$\frac{2}{\big(1+\alpha\big)\sqrt{2/3}\,\|\boldsymbol{s}\|}\left[t_m^2 - \frac{4\alpha^2-1}{4\big(1-\alpha^2\big)}t_n^2 + \frac{\alpha}{1-\alpha}qt_n - \frac{1+\alpha}{3\big(1-\alpha\big)}q^2\right] \le 0 \tag{C.4}$$

which can be transformed into the homogeneous failure function (4.34) of degree $M = 2$.

In the case of plane strain, the discontinuity angle (4.43) leads to the following normal traction t_n

$$t_n = \sigma_1 + \sigma_2 - \sigma_3 = \frac{\big(1-4\alpha^2\big)\big(\sigma_1+\sigma_2\big) + 2\alpha\big(1+\alpha\big)q}{2\big(1-\alpha^2\big)} \tag{C.5}$$

which yields the following relations

$$\sigma_1 + \sigma_2 = \frac{2\big(1-\alpha^2\big)t_n - 2\alpha\big(1+\alpha\big)q}{1-4\alpha^2} \tag{C.6a}$$

$$\sigma_3 = \frac{\left(1+2\alpha^2\right)t_n - 2\alpha\left(1+\alpha\right)q}{1-4\alpha^2} \tag{C.6b}$$

Similarly, the square of the tangential traction t_m^2 is given by

$$t_m^2 = -\left(2s_1+s_2\right)\left(s_1+2s_2\right) \tag{C.7}$$

Accordingly, the normal and tangential components (γ_n, γ_m) are evaluated from Eq. (4.6) as

$$\gamma_n = \frac{3\alpha}{1+\alpha}, \qquad \gamma_m = \frac{2\alpha}{1+\alpha}\cdot\frac{t_m}{s_1+s_2} \tag{C.8}$$

where the following relation applies

$$s_1+s_2 = \frac{\sigma_1+\sigma_2-2\sigma_3}{3} = \frac{2\alpha}{3\left(1-4\alpha^2\right)}\left[-3\alpha t_n + \left(1+\alpha\right)q\right] \geq 0 \tag{C.9}$$

owing to the relation (4.42). It then follows from Eq. (4.7) that

$$f(\boldsymbol{t},q) = \frac{1}{1+\alpha}\left[\frac{3\left(1-4\alpha^2\right)}{\left(1+\alpha\right)q-3\alpha t_n}t_m^2 - 3\alpha t_n + \left(1+\alpha\right)q\right] \leq 0 \tag{C.10}$$

which can be transformed into the form (4.46).

References

Abu Al-Rub, R.K., Darabi, M.K., 2012. A thermodynamic framework for constitutive modeling of time- and rate-dependent materials. Part I: Theory. Int. J. Plast. 34, 61–92.

Armero, F., 1999. Large-scale modeling of localized dissipative mechanisms in a local continuum: applications to the numerical simulation of strain localization in rate-dependent inelastic solids. Mech. Cohes. Frict. Mater. 4, 101–131.

Armero, F., Kim, J., 2012. Three-dimensional finite elements with embedded strong discontinuities to model material failure in the infinitesimal range. Int. J. Numer. Methods Eng. 91, 1291–1330.

Armero, F., Oller, S., 2000. A general framework for continuum damage models. i: Infinitesimal plastic damage models in stress space. Int. J. Solids Struct. 37, 7409–7464.

Barenblatt, G.I., 1959. The formation of equilibrium cracks during brittle fracture. general ideas and hypotheses. axially-symmetric cracks. J. Appl. Math. Mech. 23, 622–636.

Bažant, Z.P., Oh, B.H., 1983. Crack band theory for fracture of concrete. In: Materials and Structures, vol. 16. RILEM, Paris, pp. 155–177.

Besson, J., Steglich, D., Brocks, W., 2003. Modeling of plane strain ductile rupture. Int. J. Plast. 19, 1517–1541.

Borré, G., Maier, G., 1989. On linear versus nonlinear flow rules in strain localization analysis. Meccanica 24, 36–41.

Carol, I., Prat, P., López, C., 1997. Normal/shear cracking model: Application to discrete crack analysis. J. Eng. Mech. ASCE 123 (8), 765–773.

Carol, I., Rizzi, E., Willam, K., 1994. A unified theory of elastic degradation and damage based on a loading surface. Int. J. Solids Struct. 31 (20), 2835–2865.

Cervera, M., Chiumenti, M., Benedetti, L., Codina, R., 2015. Mixed stabilized finite element methods in nonlinear solid mechanics. part III: Compressible and incompressible plasticity. Comput. Methods Appl. Mech. Eng. 285, 752–775.

Cervera, M., Chiumenti, M., Di Capua, D., 2012. Benchmarking on bifurcation and localization in j_2 plasticity for plane stress and plane strain conditions. Comput. Methods Appl. Mech. Eng. 241–244, 206–224.

Cervera, M., Wu, J.Y., 2015. On the conformity of strong, regularized, embedded and smeared discontinuity approaches for the modeling of localized failure in solids. Int. J. Solids Struct. 71, 19–38.

Chaboche, J.L., 2008. A review of some plasticity and viscoplasticity constitutive theories. Int. J. Plast. 24, 1642–1693.

Chen, W.F., 1994. Constitutive Equations for Engineering Materials: Plasticity and Modeling #2. Elsevier, Amsterdam.

Dugdale, D., 1960. Yielding of steel sheets containing slits. J. Mech. Phys. Solids 8, 100–108.

Dumstorff, P., Meschke, G., 2006. Crack propagation criteria in the framework of x-FEM-based structural analysis. Int. J. Numer. Anal. Methods Geomech. 31, 239–259.

Hansbo, A., Hansbo, P., 2004. A finite element method for the simulation of strong and weak discontinuities in solid mechanics. Comput. Methods Appl. Mech. Eng. 193, 3523–3540.

Hill, R., 1958. General theory of uniqueness and stability of elasto-plastic solids. J. Mech. Phys. Solids 6, 236–249.

Hill, R., 1962. Acceleration waves in solids. J. Mech. Phys. Solids 10, 1–16.

Hillerborg, A., Modeer, M., Petersson, P.E., 1976. Analysis of crack formation and crack growth in concrete by means of fracture mechanics and finite elements. Cem. Concr. Res. 6, 773–782.

Horstemeyer, M.F., Bammann, D.J., 2010. Historical review of internal state variable theory for inelasticity. Int. J. Plast. 26, 1310–1334.

Huespe, A.E., Needleman, A., Oliver, J., Sánchez, P.J., 2009. A finite thickness band method for ductile fracture analysis. Int. J. Plast. 25, 2349–2365.

Huespe, A.E., Needleman, A., Oliver, J., Sánchez, P.J., 2012. A finite strain, finite band method for modeling ductile fracture. Int. J. Plast. 28, 53–69.

Ibrahimbegovic, A., 2009. Nonlinear Solid Mechanics: Theoretical Formulations and Finite Element Solution Methods. Springer, New York.

Ibrahimbegovic, A., Jehel, P., Davennel, L., 2008. Coupled damage-plastic constitutive model and direct stress interpolation. Comput. Mech. 42 (1), 1–11.

Itskov, M., 2007. Tensor Algebra and Tensor Analysis for Engineers: With Applications to Continuum Mechanics. Springer, Berlin.

Jirásek, M., Rolshoven, S., 2009. Localization properties of strain-softening gradient plasticity models. part i: strain-gradient theories. Int. J. Solids Struct. 46 (11–12), 2225–2238.

Jirásek, M., Zimmermann, T., 2001. Embedded crack model. part II: Combination with smeared cracks. Int. J. Numer. Methods Eng. 50 (6), 1291–1305.

Ju, J.W., 1989. On energy-based coupled elastoplastic damage theories: constitutive modeling and computation aspects. Int. J. Solids Struct. 25, 803–833.

Krajcinovic, D., 2003. Damage Mechanics. Elsevier B. V., Netherlands.

Lemaitre, J., 1996. A Course on Damage Mechanics. Springer, Berlin.

Lubarda, V.A., 2002. Elastoplasticity Theory. CRC Press, New York.

Meschke, G., Lackner, R., Mang, H.A., 1998. An anisotropic elastoplastic damage model for plain concrete. Int. J. Numer. Methods Eng. 42, 703–727.

Mohr, O., 1900. Welche umstände bedingen die elastizitätsgrenze und den bruch eines materials? Civilingenieur: Zeitschrift des Vereins deutscher Ingenieure VDI 44/45, 1524–1530.1572–1577.

Mosler, J., 2005. On advanced solution strategies to overcome locking effects in strong discontinuity approaches. Int. J. Numer. Methods Eng. 63, 1313–1341.

Most, T., Bucher, C., 2007. Energy-based simulation of concrete cracking using an improved mixed-mode cohesive crack model within a meshless discretization. Int. J. Numer. Anal. Methods Geomech. 31, 285–305.

Ngo, D., Scordelis, A.C., 1967. Finite element analysis of reinforced concrete beams. ACI J. 64 (14), 152–163.

Oliver, J., 1996. Modeling strong discontinuities in solid mechanics via strain softening contitutive equations. part i: Fundaments & part II: Numerical simulation. Int. J. Numer. Methods Eng. 39, 3575–3623.

Oliver, J., 2000. On the discrete constitutive models induced by strong discontinuity kinematics and continuum constitutive equations. Int. J. Solids Struct. 37, 7207–7229.

Oliver, J., Cervera, M., Manzoli, O., 1998. On the use of strain-softening models for the simulation of strong discontinuities in solids. Material Instabilities in Solids. Wiley, pp. 107–123.

Oliver, J., Cervera, M., Manzoli, O., 1999. Strong discontinuities and continuum plasticity models: the strong discontinuity approach. Int. J. Plast. 15, 319–351.

Oliver, J., Huespe, A.E., Dias, I.F., 2012. Strain localization, strong discontinuities and material fracture: Matches and mismatches. Comput. Methods Appl. Mech. Eng. 241–244, 323–336.

Oliver, J., Huespe, A.E., Pulido, M.D.G., Blanco, S., Linero, D., 2006a. On the fracture models determined by the continuum-strong discontinuity approach. Int. J. Fract. 137, 211–229.

Oliver, J., Huespe, A.E., Pulido, M.D.G., Chaves, E., 2002. From continuum mechanics to fracture mechanics: the strong discontinuity approach. Eng. Fract. Mech. 69, 113–136.

Oliver, J., Huespe, A.E., Sànchez, P.J., 2006b. A comparative study on finite elements for capturing strong discontinuities: E-FEM vs x-FEM. Comput. Methods Appl. Mech. Eng. 195, 4732–4752.

Ortiz., M., 1985. A constitutive theory for the inelastic behavior of concrete. Mech. Mater. 4, 76–93.

Ottosen, N., Runesson, K., 1991. Discontinuous bifurcations in a non-associated Mohr material. Mech. Mater. 12, 255–265.

Rashid, Y., 1968. Analysis of prestressed concrete pressure vessels. Nucl. Eng. Des. 7, 334–344.

Remmers, J.J.C., de Borst, R., Verhoosel, C.V., Needleman, A., 2013. The cohesive band model: a cohesive surface formulation with stress triaxiality. Int. J. Fract. 181, 177–188.

Rice, J.R., Rudnicki, J.W., 1980. A note on some features of the theory of localization of deformation. Int. J. Solids Struct. 16, 597–605.

Roscoe, K.H., 1970. The influence of strains in soil mechanics, 10th rankine lecture. Géotechnique 20, 129–180.

Rots, J.G., 1988. Computational Modeling of Concrete Fracture. Delft University of Technology, Delft, The Netherlands Doctoral dissertation.

Rudnicki, J.W., Rice, J.R., 1975. Conditions of the localization of deformation in pressure-sensitive dilatant material. J. Mech. Phys. Solids 23, 371–394.

Runesson, K., Ottosen, N.S., Peric, D., 1991. Discontinuous bifurcations of elastic-plastic solutions at plane stress and plane strain. Int. J. Plast. 7, 99–121.

Sánchez, P.J., Huespe, A.E., Oliver, J., 2008. On some topics for the numerical simulation of ductile fracture. Int. J. Plast. 24, 1008–1038.

Simó, J.C., Oliver, J., Armero, F., 1993. An analysis of strong discontinuities induced by strain-softening in rate-independent inelastic solids. Comput. Mech. 12, 277–296.

Svedberg, T., Runesson, K., 1997. A thermodynamically consistent theory of gradient-regularized plasticity coupled to damage. Int. J. Plast. 13, 669–696.

Thomas, T.Y., 1961. Plastic Flow and Fracture of Solids. Academic Press, New York.

Voyiadjis, G.Z., Alsaleh, M.I., Alshibli, K.A., 2005. Evolving internal length scales in plastic strain localization for granular materials. Int. J. Plast. 21, 2000–2024.

Voyiadjis, G.Z., Dorgan, R.J., 2007. Framework using functional forms of hardening internal state variables in modeling elasto-plastic-damage behavior. Int. J. Plast. 23, 1826–1859.
Voyiadjis, G.Z., Kattan, P.I., 1992. A plasticity-damage theory for large deformation of solids. part i: Theoretical formulation. Int. J. Eng. Sci. 30 (9), 1089–1108.
Vrech, S., Etse, G., 2005. Geometrical localization analysis of gradient-dependent parabolic Drucker-Prager elastoplasticity. Int. J. Plast. 22 (5), 943–964.
Wells, G.N., Sluys, L.J., 2001. A new method for modelling cohesive cracks using finite elements. Int. J. Numer. Meth. Eng. 50, 2667–2682.
Wu, J.Y., 2011. Unified analysis of enriched finite elements for modeling cohesive cracks. Comput. Methods Appl. Mech. Eng. 200 (45–46), 3031–3050.
Wu, J.Y., Cervera, M., 2013. Strain localization in elastoplastic damage solids. In: Proceedings of the International Symposium on Innovation and Sustainability of Structures in Civil Engineering (ISISS-2013), Harbin, China.
Wu, J.Y., Cervera, M., 2014a. On the stress continuity condition for strain localization in softening solids. In: Proceedings of the Eleventh World Congress On Computational Mechanics (WCCM-2014), Barcelona, Spain.
Wu, J.Y., Cervera, M., 2014b. Strain localization and failure mechanics for elastoplastic damage solids. In: Proceedings of the Monograph CIMNE, M147, Barcelona, Spain.
Wu, J.Y., Cervera, M., 2015. On the equivalence between traction- and stress-based approached for the modeling of localized failure in solids. J. Mech. Phys. Solids 82, 137–163.
Wu, J.Y., Li, F.B., 2015. An improved stable XFEM (is-XFEM) with a novel enrichment function for the computational modeling of cohesive cracks. Comput. Methods Appl. Mech. Eng. 295, 77–107.
Wu, J.Y., Li, F.B., Xu, S.L., 2015. Extended embedded finite elements with continuous displacement jumps for the modeling of localized failure in solids. Comput. Methods Appl. Mech. Eng. 285, 346–378.
Wu, J.Y., Li, J., Faria, R., 2006. An energy release rate-based plastic-damage model for concrete. Int. J. Solids Struct. 43 (3–4), 583–612.
Wu, J.Y., Xu, S.L., 2011. An augmented multicrack elastoplastic damage model for tensile cracking. Int. J. Solids Struct. 48, 2511–2528.
Wu, J.Y., Xu, S.L., 2013. Reconsideration on the elastic damage/degradation theory for the modeling of microcrack closure-reopening (MCR) effects. Int. J. Solids Struct. 50 (5), 795–805.
Zhu, Y., Sun, L., Zhu, H., 2010. A coupled damage and plasticity Drucker-Prager model based on thermodynamics of internal variables. GeoFlorida 2010, 139–146.